Electronic Supplementary Information

Experimental section

Materials. Zinc nitrate hexahydrate ($Zn(NO_3)_2·6H_2O$), 2-methylimidazole (MeIM), Iron(Ⅲ) nitrate nonahydrate ($Fe(NO_3)_3·9H_2O$), Copper(II) phthalocyanine (CuPc) Potassium nitrate (KNO_3), potassium nitrate-^{15}N ($K^{15}NO_3$), and deuterium oxide (D_2O, 99.9 atom% D) were obtained from the Shanghai Macklin Biochemical Co., Ltd. Ethanol (C_2H_5OH), sodium hydroxide (NaOH), methanol, hydrochloric acid (HCl), and potassium hydroxide (KOH) were purchased from Tianjin Yuanli Company (Tianjin, China). Sodium nitroferricyanide (III) dihydrate ($Na_2Fe(CN)_5NO·2H_2O$), para-(dimethylamino) benzaldehyde ($C_9H_{11}NO$), sodium hypochlorite (NaClO), maleic acid ($C_4H_4O_4$), sodium citrate ($C_6H_5Na_3O_7$), and salicylic acid ($C_7H_6O_3$) were obtained from Aladdin Ltd. Carbon paper was bought from Beijing Chemical Corporation. Nafion solution (5 wt%) was purchased from Sigma-Aldrich Chemical Reagent Co., Ltd. Deionized water (18.2 MΩ cm) was obtained from a Millipore system.

Synthesis of N-C. In a typical procedure, 2.3 g 2-methylimidazole was ultrasonically dissolved in 50 mL methanol for 5 min, and then added into 50 mL methanol containing 1.04 g $Zn(NO_3)_2·6H_2O$ under vigorous stirring. The above solution was stirred for 24 h at room temperature. Then, The resulting precipitates were centrifuged and washed with methanol for several times and dried in vacuum at 70 ℃ overnight. Finally, The collected sample was placed in a tube furnace and heat-treated to 1000 ℃ for 3 h at a heating rate of 5 ℃/min in Ar atmosphere to obtain N-C.

Synthesis of Cu-Fe-N-C. In a typical procedure, 2.3 g 2-methylimidazole and 20 mg CuPc were ultrasonically dissolved in 50 mL methanol for 5 min, and then added into 50 mL methanol containing 1.04 g $Zn(NO_3)_2·6H_2O$ and 20 mg $Fe(NO_3)_3·9H_2O$ under vigorous stirring. The above solution was stirred for 24 h at room temperature. Then, The resulting precipitates were centrifuged and washed with methanol for several times and dried in vacuum at 70 ℃ overnight. Finally, The collected sample was placed in a tube furnace and heat-treated to 1000 ℃ for 3 h at a heating rate of 5 ℃/min in Ar atmosphere to obtain Cu-Fe-N-C.

Synthesis of Cu-N-C. Cu-N-C was synthesized using the similar method as Cu-Fe-N-C except that there was no added $Fe(NO_3)_3·9H_2O$.

Synthesis of Fe-N-C. Fe-N-C was synthesized using the similar method as Cu-Fe-N-C except that there was no added CuPc.

Characterization. The X-ray diffraction (XRD) patterns were obtained from a D8-Focus X-ray diffractometer (BRUKER AXS GMBH) equipped with Cu Kα radiation at 40 kV and 40 mA. Scanning electron microscopy (SEM) images were collected from a S-4800 scanning electron microscope. Transmission electron microscopy (TEM) images were performed on a Tecnai G2F-20 microscope with a field-emission gun, operated at 200 kV. High-angle annular dark field-scanning transmission electron microscopy (HAADF-STEM) measurements were carried out on a ARM200F. The X-ray photoelectron spectroscopy (XPS) spectra were performed using a PHI-1600 X-ray photoelectron spectrometer equipped with Al Kα radiation. Binding energy was calibrated to the C1s feature located at 284.8 eV. The absorbance data of spectrophotometer were measured on SHIMADZU UV-1800 ultraviolet-visible (UV-Vis) spectrophotometer. In situ Fourier transform infrared (FTIR) spectroscopy were measured with a BRUKER TENSOR FTIR spectrometer. The online differential electrochemical mass spectrometry (DEMS) (QAS 100, Linglu instruments (Shanghai) Co. Ltd) measurements were collected to capture the intermediates. ^1H nuclear magnetic resonance (NMR) spectra were collected on JEOL JNM ECZ600R.

Electrochemical NO_3RR measurements. The electrochemical tests were carried out using corrtest electrochemical workstation on a three-electrode configuration H-type cell. To prepare the work cathode, 5 mg obtained catalysis were dissolved in 960 μL ethanol and 40 μL of Nafion solution (5wt%) ultrasonically for at least 1 h to form a homogeneous ink. Then, 40 μL of catalyst ink was loaded onto a carbon paper with area of 1 ×0.5 cm^2 with a mass loading of 0.4 mg cm^{-2} and dried under ambient conditions. Pt slice and Hg/HgO were used as counter electrode and reference electrode, respectively. The electrolyte in both the cathode and anode chamber were made up of 1 M KOH with 0.1 M KNO_3. All potentials were converted to the reversible hydrogen electrode (RHE) scale via calibration (E(RHE)= E (Hg/HgO) + 0.098 V + 0.059 × pH. Prior to each measurement, the electrolyte was purged with Ar gas for at least 30 minutes to remove O_2 and N_2. The linear sweep voltammetry (LSV) tests were scanned at a rate of 10 mV s^{-1}. The potentiostatic tests were operated at different potentials for 30 min. The electrolyte in cathodic compartment was stirred with a rate of 600 rpm. The long-term performance of the Cu-Fe-N-C catalysts was evaluated at -0.8 V vs. RHE, in which the 5 L electrolyte with flow rate of 10 mL min^{-1}. The electroreduction reaction maintained 50 h electrolysis each time. The cyclic voltammograms (CV) were perfromed at different scan rate (10, 20, 30, 40, 50, 60 mV s^{-1}) to obtain the double-layer capacitance (C_{dl}). The C_{dl} was recorded by plotting ΔJ against the scan rate.

^{15}N isotope labelling experiments and quantification by ^1H nuclear magnetic resonance (NMR). To determine the NH_3 yield rate by ^1H NMR, a calibration curve was made using a series of standard $^{15}NH_4Cl$ solutions. For $K^{15}NO_3$ isotope labelling experiment, the $K^{15}NO_3$ was chose rather than $K^{14}NO_3$. After NO_3RR electroreduction, the pH value of the electrolyte after reaction was adjusted to acidic with external standard of maleic

acid. Typically, 0.5 mL above mixture and 50 μL of D_2O were added to the NMR tube for the further analysis using ^1H NMR (600 MHz). The ratio of the peak area of $^{15}NH_4^+$ to maleic acid were determined to confirm the source of NH_3 qualitatively.

Determination of ammonia. The produced NH_3 was determined by the indophenol blue method. In detail, we took out a certain amount of electrolyte after electrochemical measurement and diluted it to the detection range. Firstly, 2 mL of the diluted electrolyte was mixed with 2 mL of 1 M NaOH solution containing salicylic acid (5 wt.%) and sodium citrate (5 wt.%). Then, 1.0 mL of NaClO solution (0.05 M), and 0.2 mL of sodium nitroferricyanide solution (1 wt.%) were added into the solution. The UV-vis absorption spectram were performed after reaction in the dark for 2 h. Finally, The concentration of NH_3 was recored using the absorbance at the wavelength of 655 nm. The calibration curve for NH_3 was measured using a set of different NH_4Cl solution as standard.

Determination of nitrite. The concentration of nitrite (NO_2^-) was determined with sulfonamide in an acidic environment, in which the diazotized compound is coupled with N-(1-naphthyl) ethylenediamine dihydrochloride. Firstly, 0.50 g of sulfanilamide was dissolved in 50.0 mL of 2.0 M HCl solution, and then 0.1 mL of the solution was mixed to 5 mL of diluted electrolyte with 10 minutes reaction at room condition. Next, 0.10 mL N-(1-Naphthyl) ethylenediamine dihydrochloride solution (1 mg/mL) was added to the solution and rested 30 minutes reaction at room condition. Finally, The absorbance at a wavelength of 540 nm was recorded to determine the concentration of NO_2^-. The calibration curve for NO_2^- was measured using a set of different KNO_2 solution as standard.

Faradaic efficiency and NH_3 yield rate. The faradaic efficiency (FE) of NH_3 and NO_2^- production was determined by the following equation:

$$FE\ (NH_3) = (8F \times C \times V) / Q$$

$$FE\ (NO_2^-) = (2F \times C \times V) / Q$$

Where F is Faraday constant (96485 C mol^{-1}), C is the measured NH_4^+ or NO_2^- concentration in the electrolyte, V is the volume of the electrolyte, Q is the the quantity of applied electricity.

The NH_3 yield rate can be calculated using the following equation:

$$NH_3\ \text{yield rate} = (C \times V) / (t \times A)$$

Where t is the electrolysis time; A is the geometric area of the electrode (0.5 cm^{-2}).

Electrochemical in situ FTIR spectrometry. In situ FTIR measurements were obtained from a BRUKER TENSOR FTIR spectrometer. The electrochemical tests were carried out in a three-electrode configuration H-type cell. The catalyst was used as the working electrode, while Pt slice and Hg/HgO were used as counter electrode and reference electrode, respectively. Before each measurement, the background spectrum of the working electrode was tested at an open circuit voltage. In situ FTIR spectra were obtained at different constant potentials.

Electrochemical online DEMS test. The DEMS measurements were obtained from a Linglu instruments. 1 M KOH with 0.1 M KNO_3 was used as electrolyte. The catalyst was used as the working electrode, while Hg/HgO and Pt wire were used as the reference and counter electrodes, respectively. Chronoamperometry at −0.8 V was performed for 60 s, which the corresponding mass signals were detected. After electrochemical test, wait for the mass signal to return to the baseline. The following cycles were carried out under the same conditions to minimize errors. The measurement was finished after four cycles.

Computational Details

All DFT calculations were performed by Vienna ab initio Simulation package (VASP) using spin-polarized density functional with the Hubbard model (DFT+U), and employing the Perdew-Burke-Ernzerhof (PBE) exchange-correlation functional with the projector augmented wave (PAW) pseudopotential method to describe interactions between the core and electrons.[1-4] Besides, the DFT-D3 method of Grimme was used for describing the long-range dispersion interaction.[5, 6] The value of the U_{eff} was fixed at 4.0 eV. [7,8] All atomic positions were fully relaxed until energy and force reached the tolerance of 1×10^{-5} eV and 0.02 eV $Å^{-1}$, respectively. A kinetic energy cut-off of 520 eV was used. The Monkhorst-Pack k-point of 2×2×1 was used to sample the Brillouin zone. All the slabs were separated by at least 15 Å of vacuum space to reduce spurious interactions between atomic layers. The following pathways are considered the most likely to occur on Cu-Fe-N-C. Involving the intermediates $*NO_3$, $*NO_3H$, $*NO_2$, $*NO_2H$, *NO, *NHO, $*NH_2O$, $*NH_2OH$, $*NH_2$ and $*NH_3$. The optimal reaction process can be represented by the following equation.

$$* + NO_3^- \rightarrow *NO_3 + e^- \quad (1)$$

$$*NO_3 + H^+ + e^- \rightarrow *NO_3H \quad (2)$$

$$*NO_3H + H^+ + e^- \rightarrow *NO_2 + H_2O \quad (3)$$

$$*NO_2 + H^+ + e^- \rightarrow *NO_2H \quad (4)$$

$$*NO_2H + H^+ + e^- \rightarrow *NO + H_2O \quad (5)$$

$$*NO + H^+ + e^- \rightarrow *NHO \quad (6)$$

$$*NHO + H^+ + e^- \rightarrow *NH_2O + H_2O \quad (7)$$

$$*NH_2O + H^+ + e^- \rightarrow *NH_2OH \quad (8)$$

$$*NH_2OH + H^+ + e^- \rightarrow *NH_2 + H_2O \quad (9)$$

$$*NH_2 + H^+ + e^- \rightarrow *NH_3 \quad (10)$$

$$*NH_3 \rightarrow * + NH_3 \quad (11)$$

where * represents the active site. The Gibbs free energy of the reaction can be calculated using the following equation.

$$\Delta G_{ads} = \Delta E_{ads} + \Delta E_{ZPE} - T\Delta S_{ads} \quad (12)$$

Where ΔE_{ads} is the electronic adsorption energy, ΔE_{ZPE} and $T\Delta S_{ads}$ are the change in zero-point energy of the adsorbates and the corresponding entropy difference. The zero point energy and entropy were obtained by calculating the vibration frequency of adsorbed molecules. To avoid the difficulties of using periodic DFT calculations for charged NO_3^-, thermodynamic cycles were used to calculate the overall free energy of NO_3^- adsorption.[9, 10]

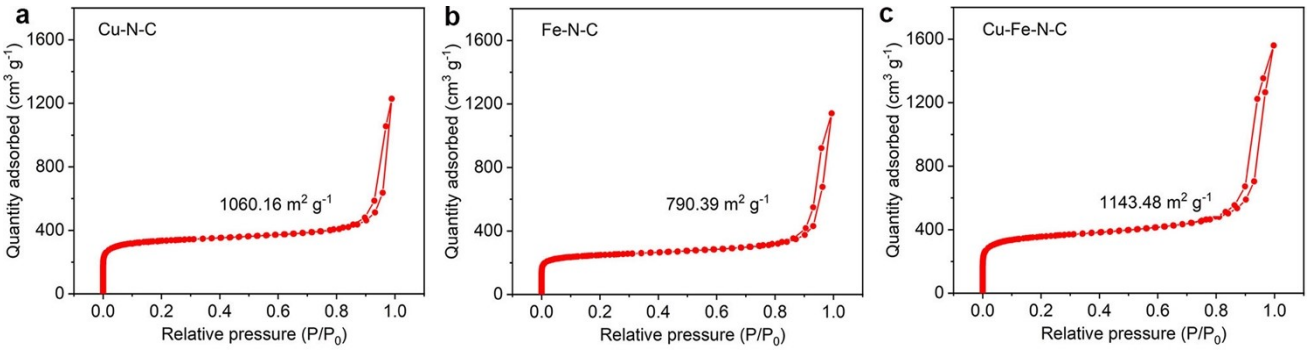

Fig. S1 N_2 adsorption-desorption isotherms curves of (a) Cu-N-C, (b) Fe-N-C, and (c) Cu-Fe-N-C.

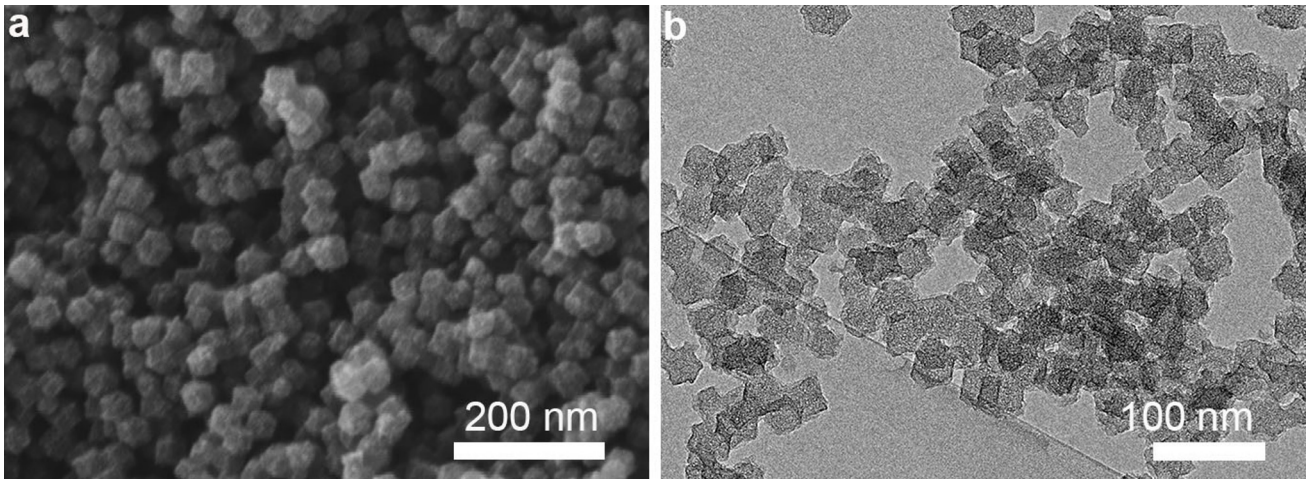

Fig. S2 (a) SEM and (b)TEM images for N-C.

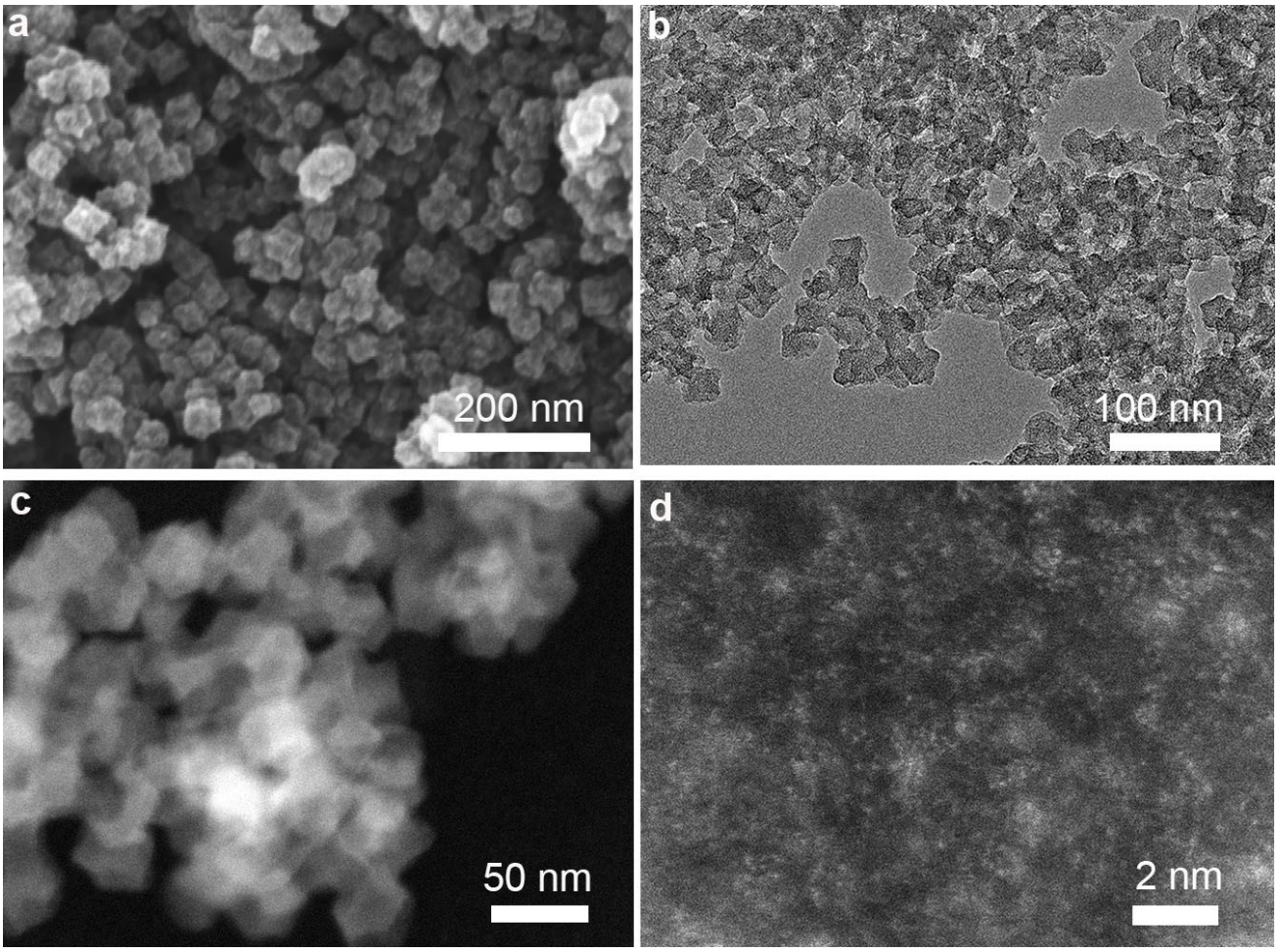

Fig. S3 (a) SEM, (b, c) TEM, and (d) HAADF-STEM images for Cu-N-C.

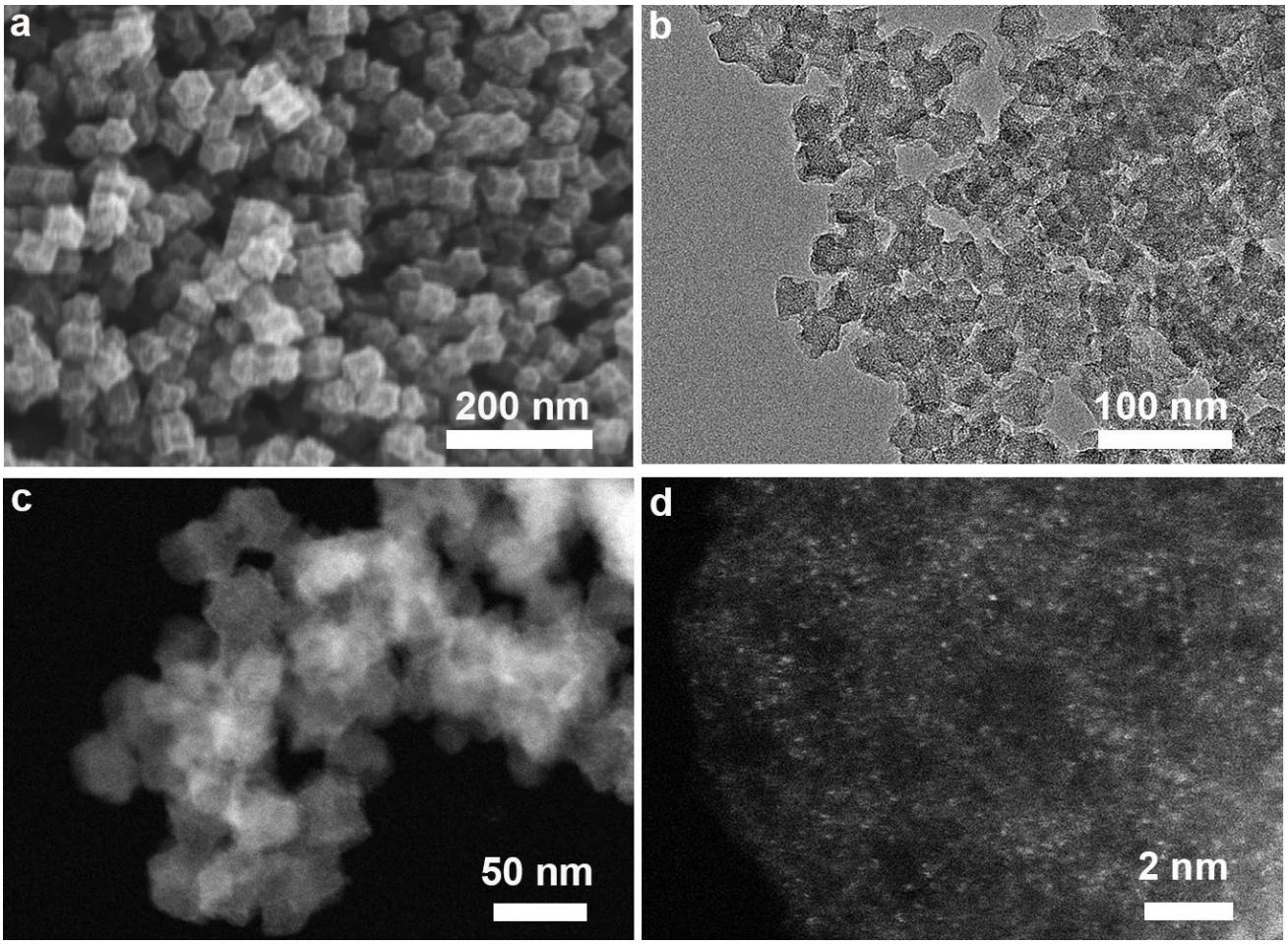

Fig. S4 (a) SEM, (b, c) TEM, and (d) HAADF-STEM images for Fe-N-C.

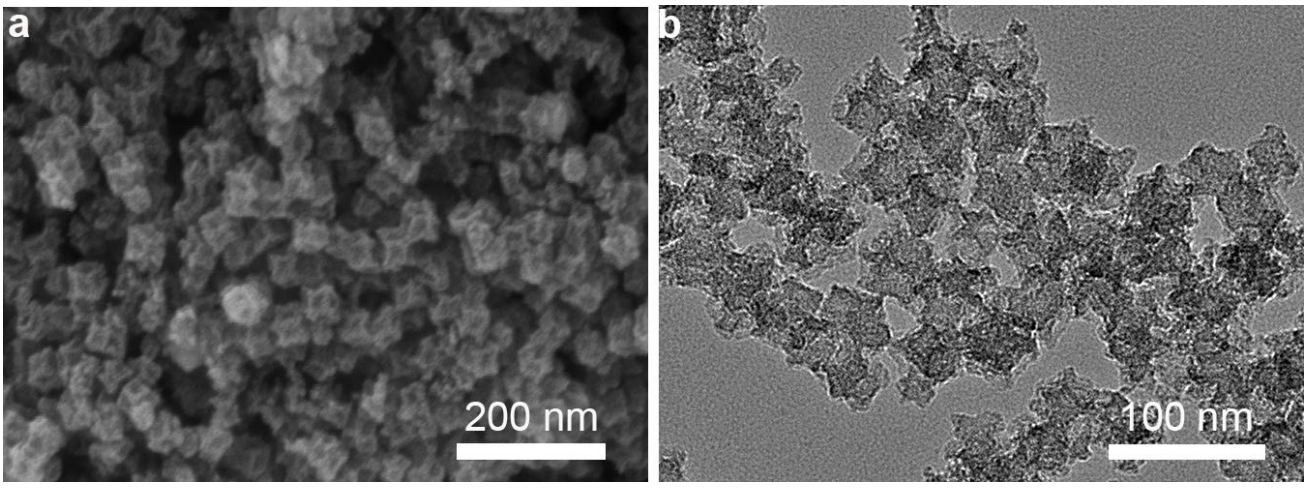

Fig. S5 (a) SEM and (b)TEM images for Cu-Fe-N-C.

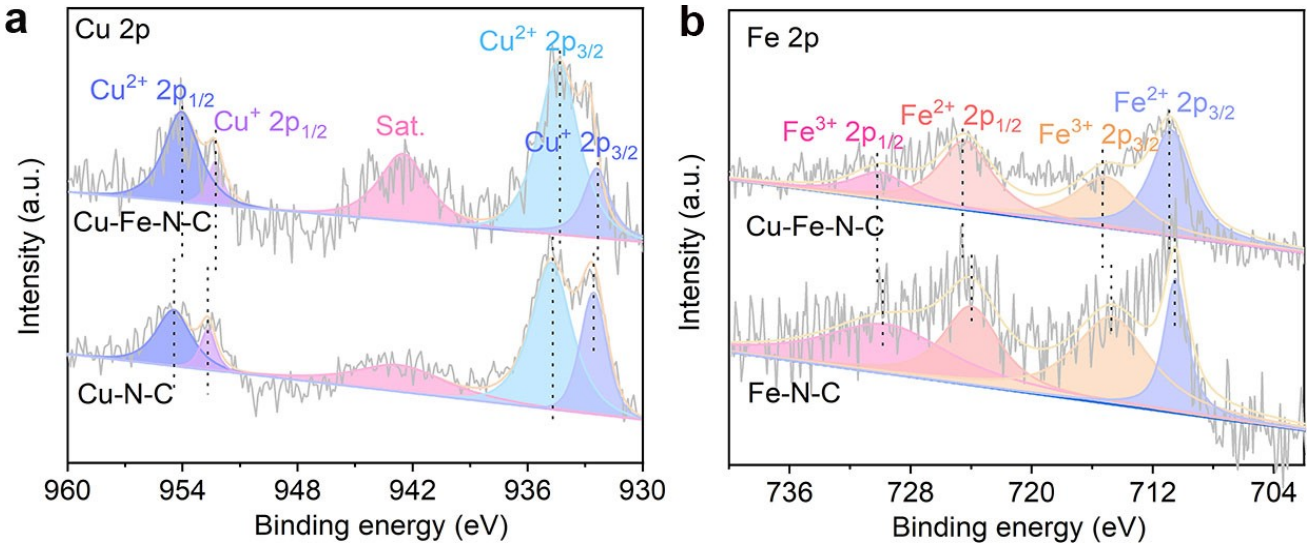

Fig. S6 XPS spectra in the (a) Cu 2p region, (b) Fe 2p region.

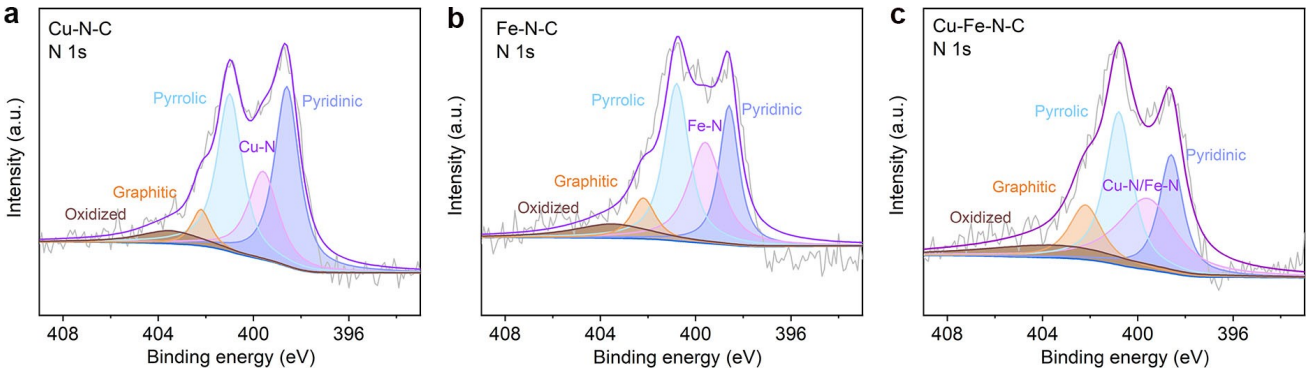

Fig. S7 XPS spectra of the (a) Cu-N-C, (b) Fe-N-C, and (c) Cu-Fe-N-C in the N 1s region.

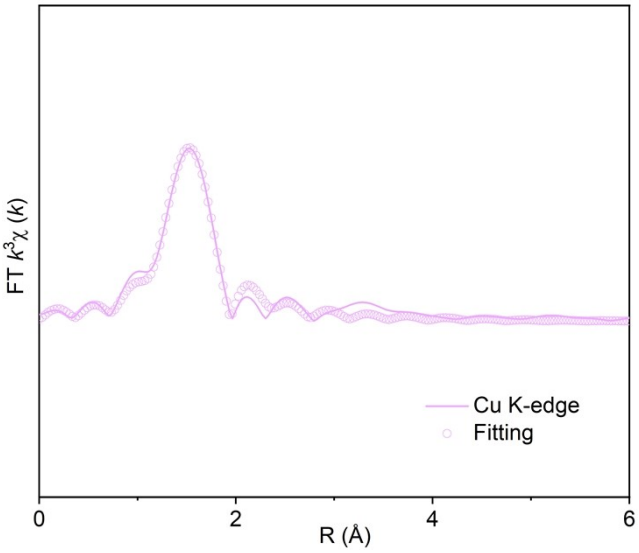

Fig. S8 The corresponding Cu K-edge EXAFS fitting for Cu-N-C.

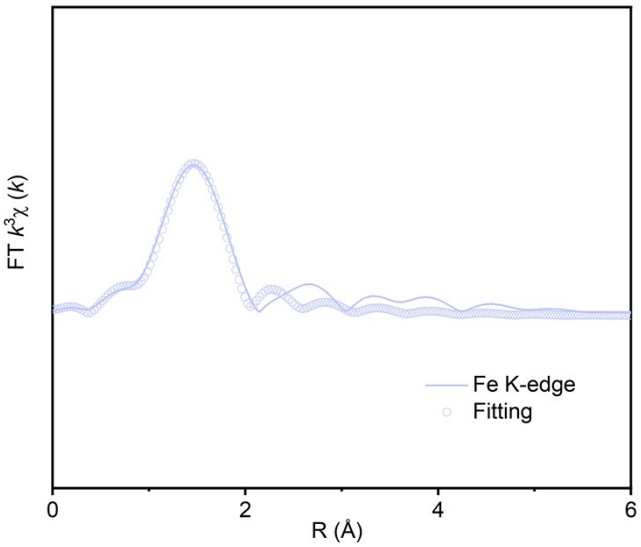

Fig. S9 The corresponding Fe K-edge EXAFS fitting for Fe-N-C.

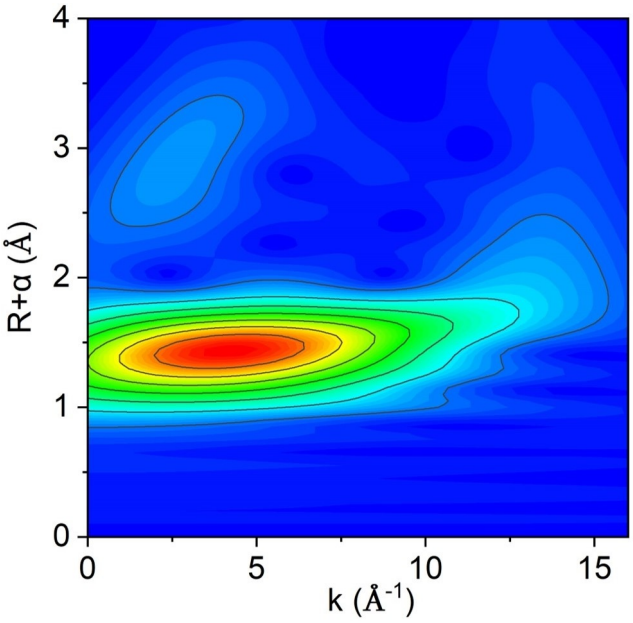

Fig. S10 The WT plots at the Cu K-edge for Cu-N-C.

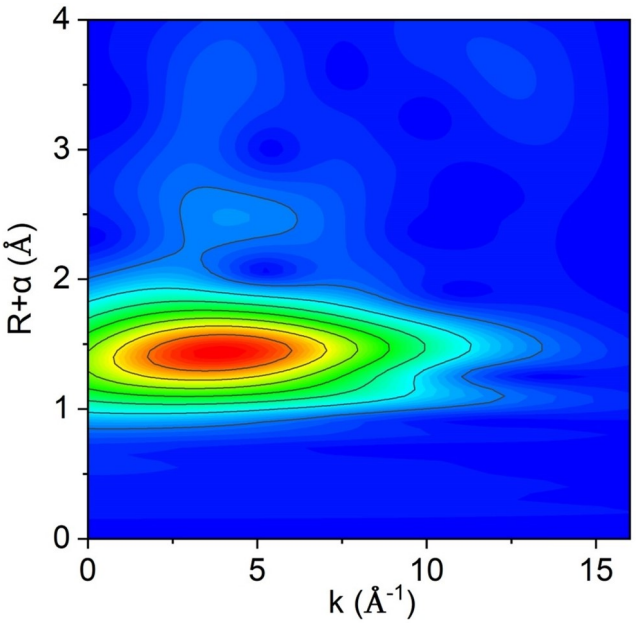

Fig. S11 The WT plots at the Fe K-edge for Fe-N-C.

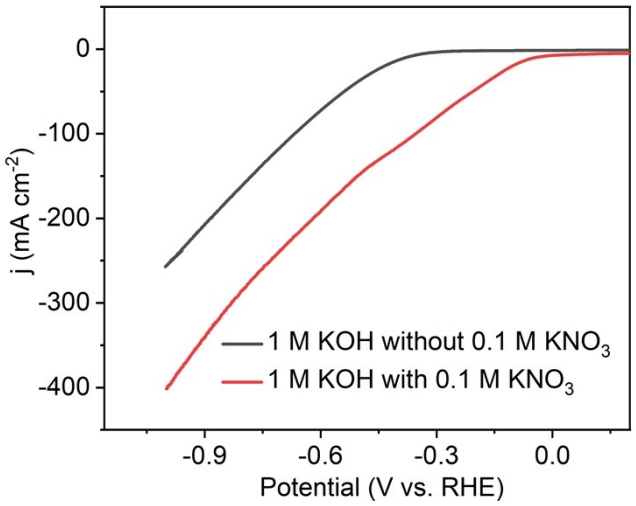

Fig. S12 The LSV curves of Cu-Fe-N-C in 1 M KOH electrolyte with and without KNO_3.

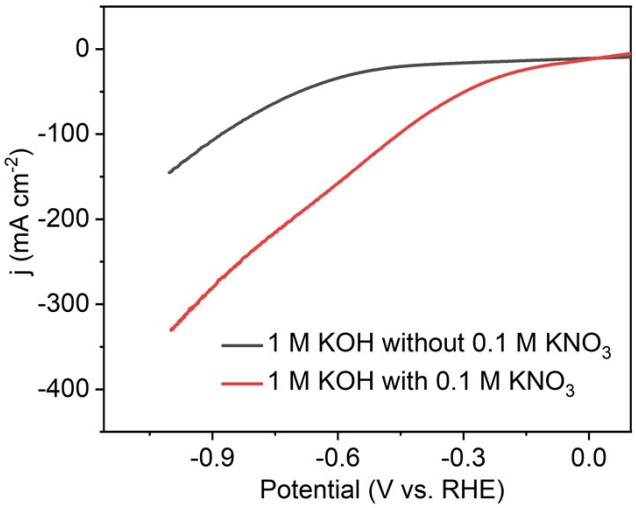

Fig. S13 The LSV curves of Cu-N-C in 1 M KOH electrolyte with and without KNO_3.

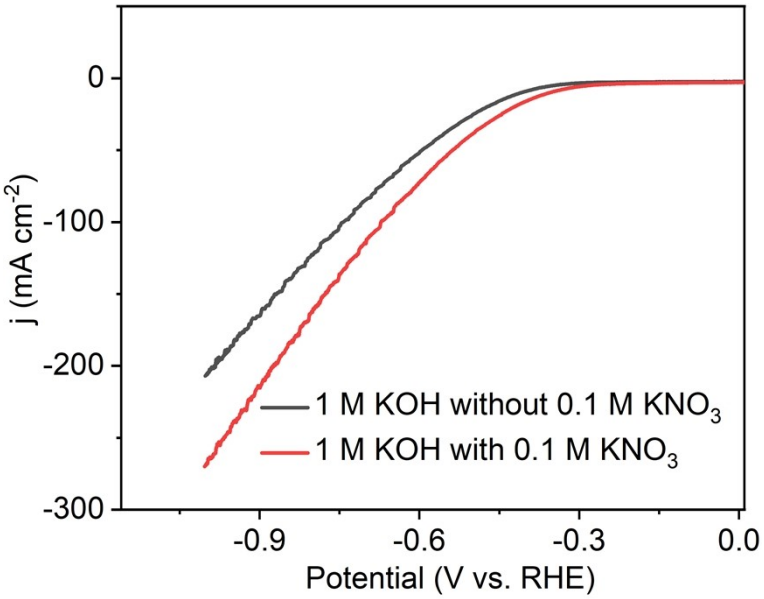

Fig. S14 The LSV curves of Fe-N-C in 1 M KOH electrolyte with and without KNO_3.

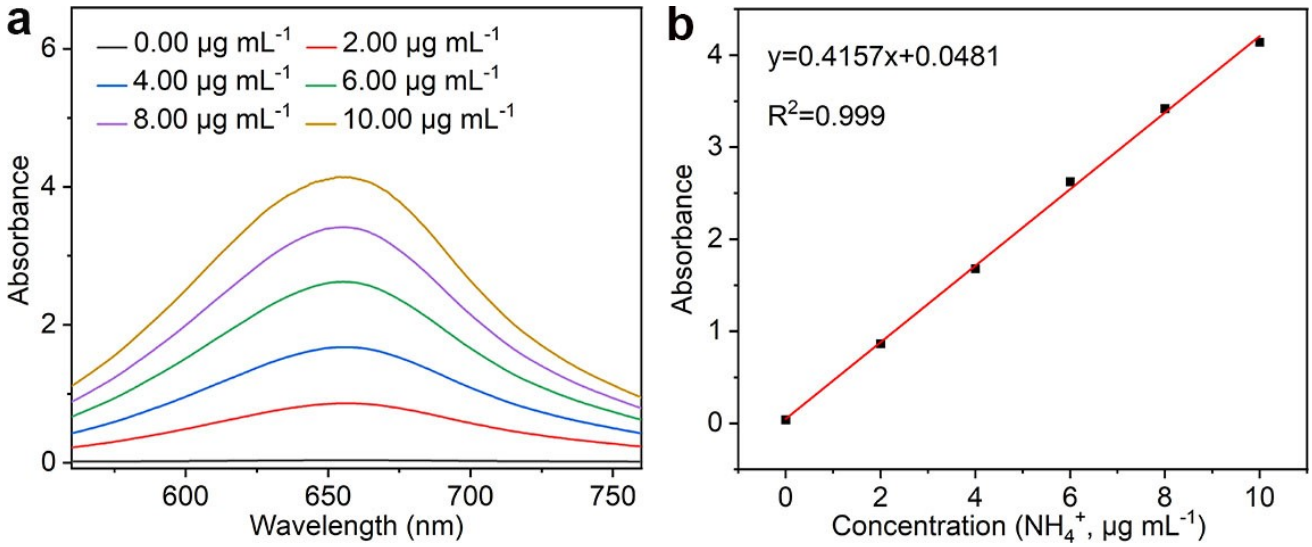

Fig. S15 (a) The UV-visible absorption spectra of various NH_4^+ concentrations. (b) The linear fitting results of NH_4^+ calibration curve.

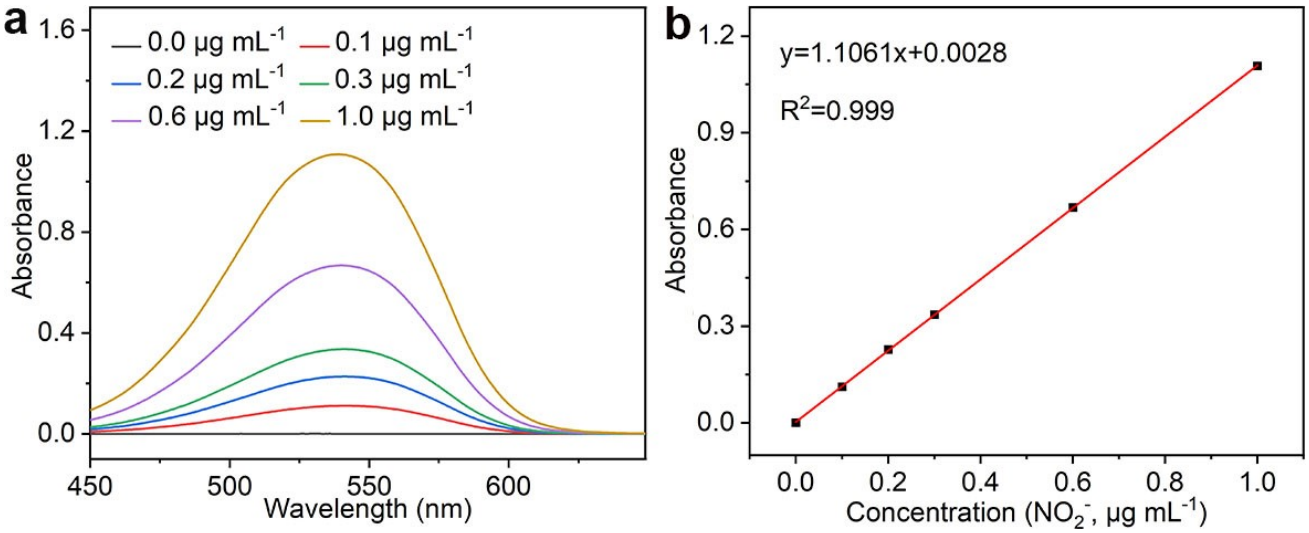

Fig. S16 (a) The UV-visible absorption spectra of various NO_2^- concentrations. (b) The linear fitting results of NO_2^- calibration curve.

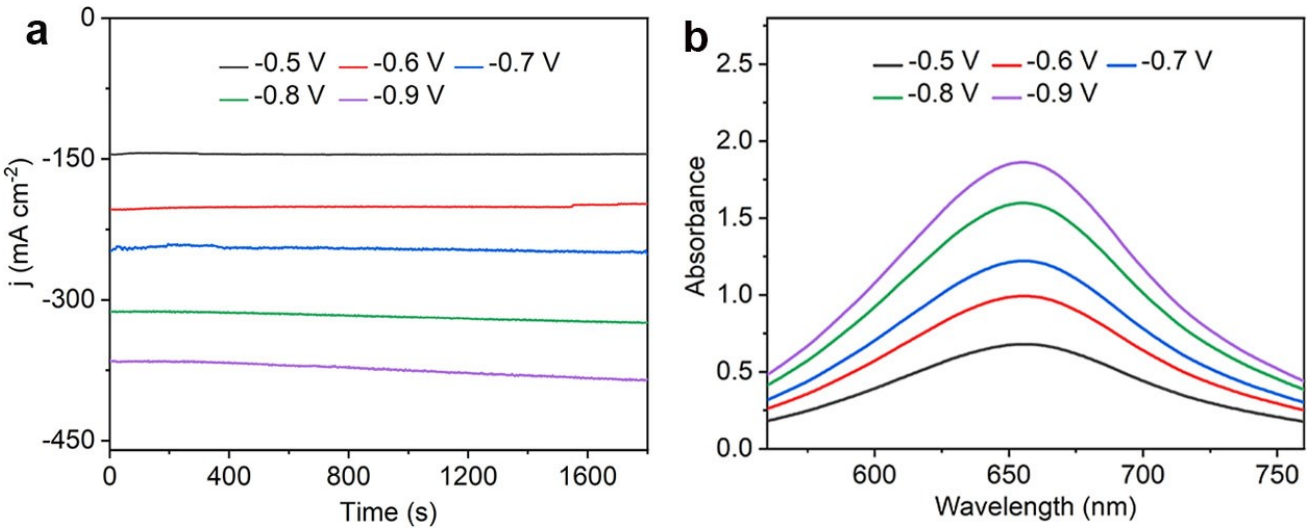

Fig. S17 (a) Time-dependent current density curves of Cu-Fe-N-C for 30 min in 1 M KOH with 0.1 M KNO_3. (b) The corresponding UV-visible absorption spectra after NO_3RR electrocatalysis.

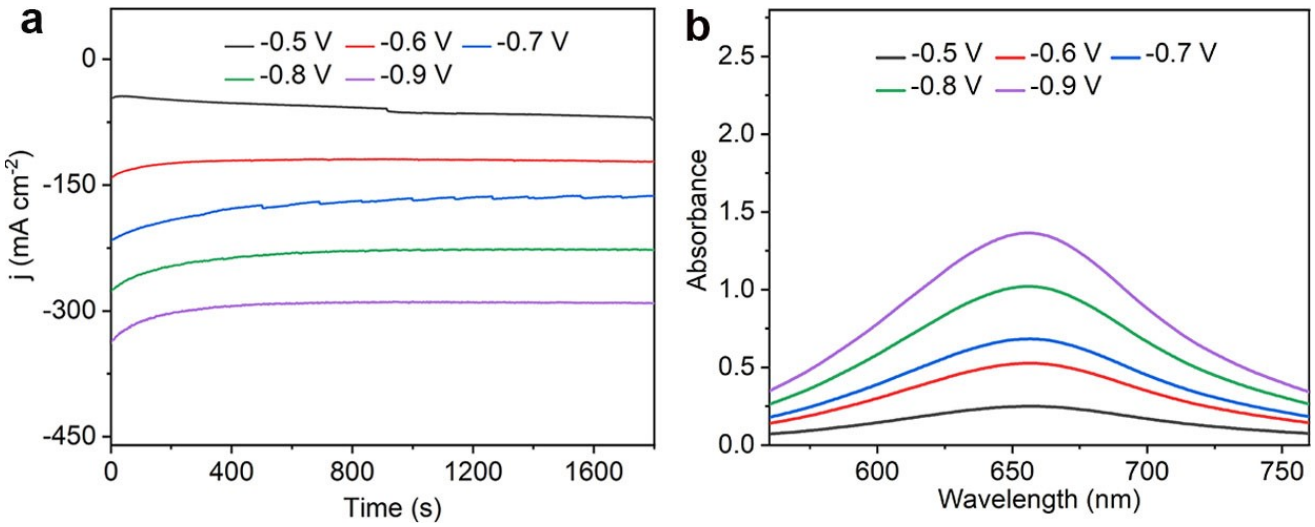

Fig. S18 (a) Time-dependent current density curves of Cu-N-C for 30 min in 1 M KOH with 0.1 M KNO_3. (b) The corresponding UV-visible absorption spectra after NO_3RR electrocatalysis.

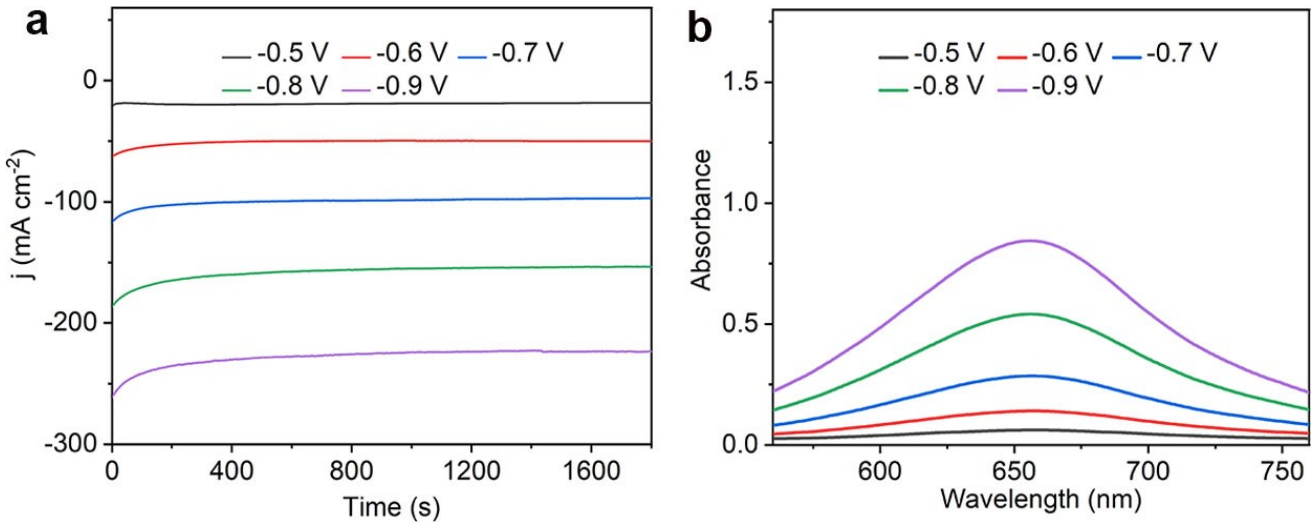

Fig. S19 (a) Time-dependent current density curves of Fe-N-C for 30 min in 1 M KOH with 0.1 M KNO_3. (b) The corresponding UV-visible absorption spectra after NO_3RR electrocatalysis.

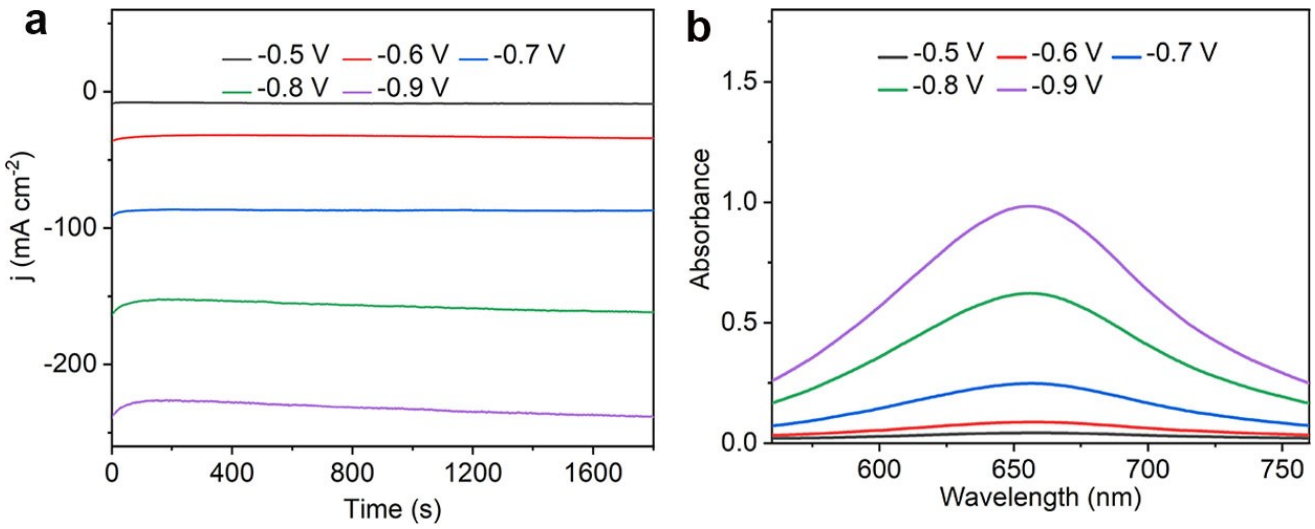

Fig. S20 (a) Time-dependent current density curves of N-C for 30 min in 1 M KOH with 0.1 M KNO_3. (b) The corresponding UV-visible absorption spectra after NO_3RR electrocatalysis.

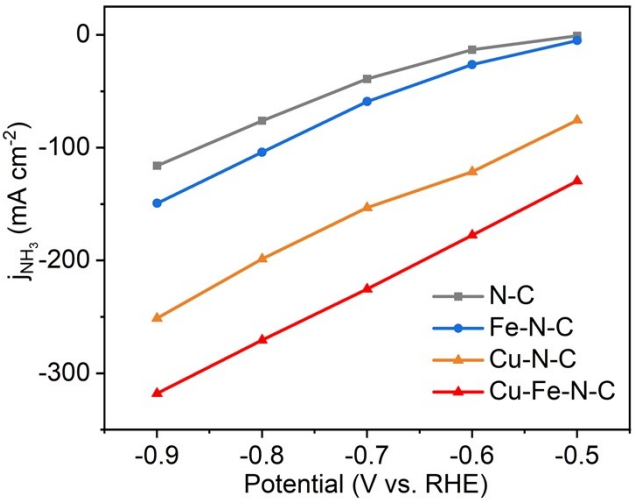

Fig. S21 j_{NH3} of Cu-Fe-N-C, Cu-N-C, Fe-N-C, and N-C in 1 M KOH with 0.1 M KNO_3.

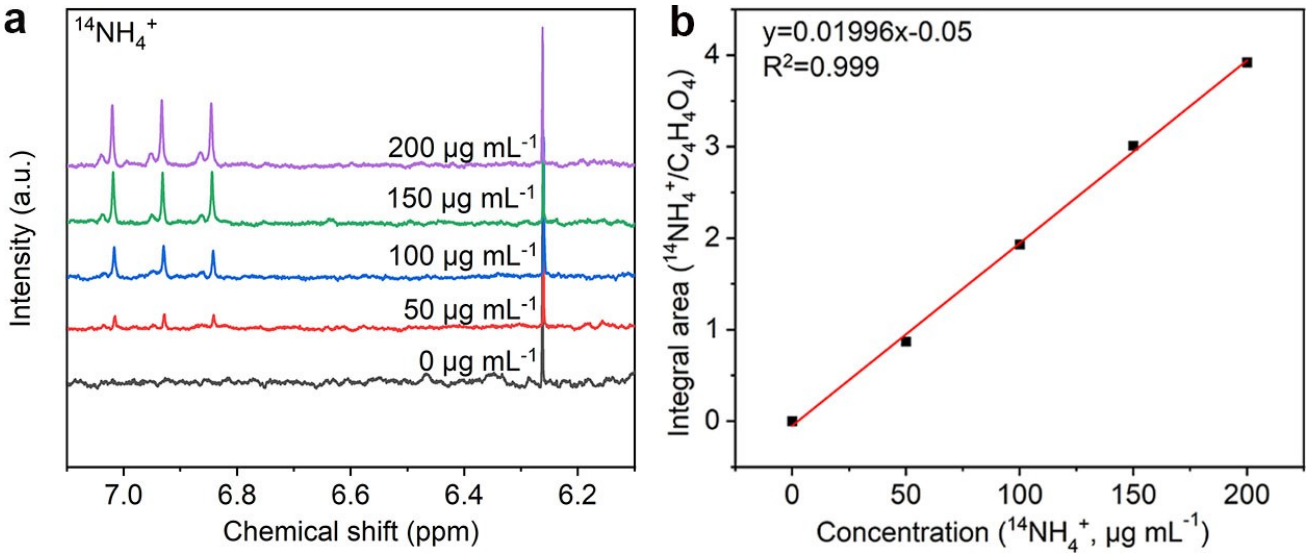

Fig. S22 (a) The ^{1}H NMR spectra of various $^{14}NH_4^+$ concentrations using maleic acid as an internal standard. (b) The linear fitting results of $^{14}NH_4^+$ calibration curve.

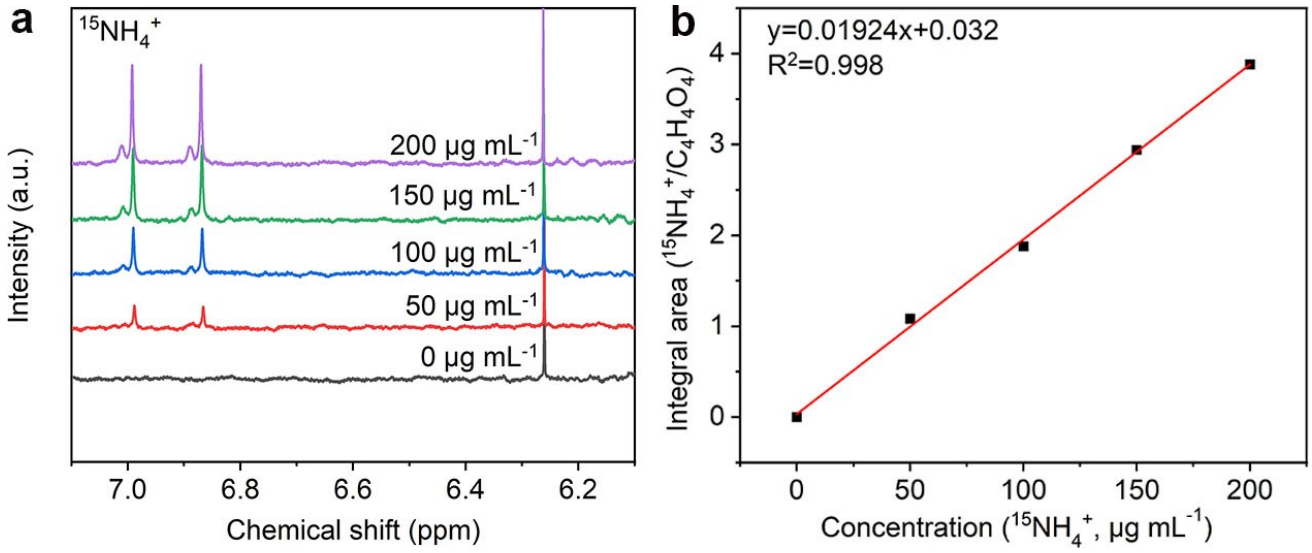

Fig. S23 (a) The ^{1}H NMR spectra of various $^{15}NH_4^+$ concentrations using maleic acid as an internal standard. (b) The linear fitting results of $^{15}NH_4^+$ calibration curve.

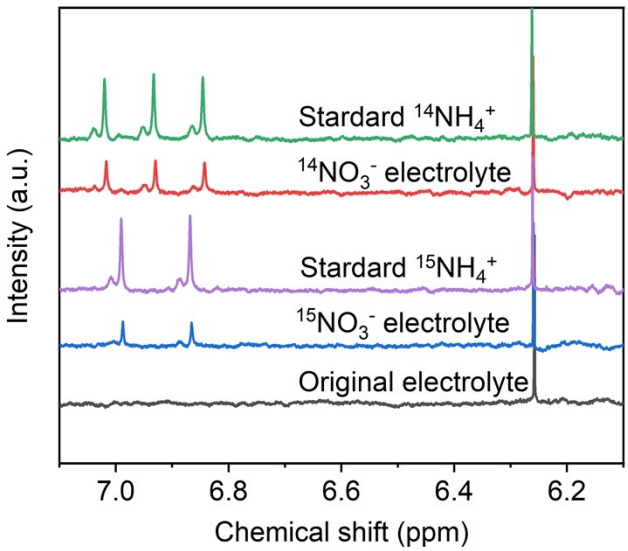

Fig. S24 The ^{1}H NMR spectra of electrolysis after electrocatalytic NO_3RR for Cu-Fe-N-C at -0.8 V using $^{14}NO_3^-$ and $^{15}NO_3^-$ as the N source.

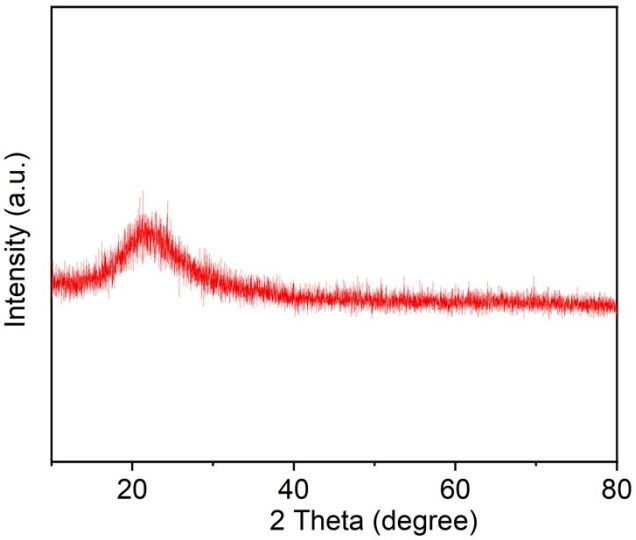

Fig. S25 XRD pattern of Cu-Fe-N-C after NO_3RR.

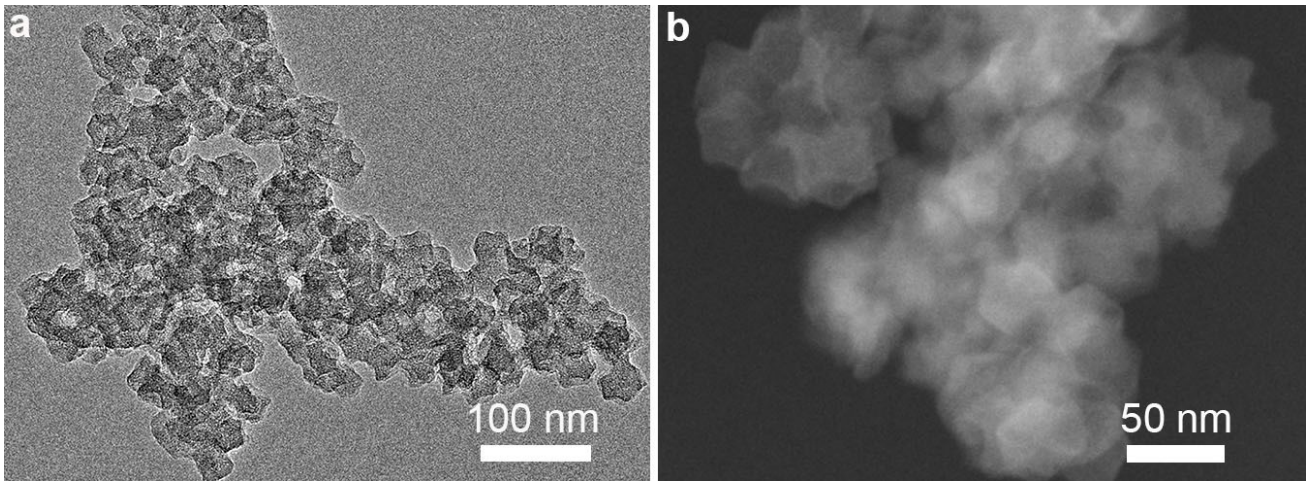

Fig. S26 TEM images of Cu-Fe-N-C after NO_3RR.

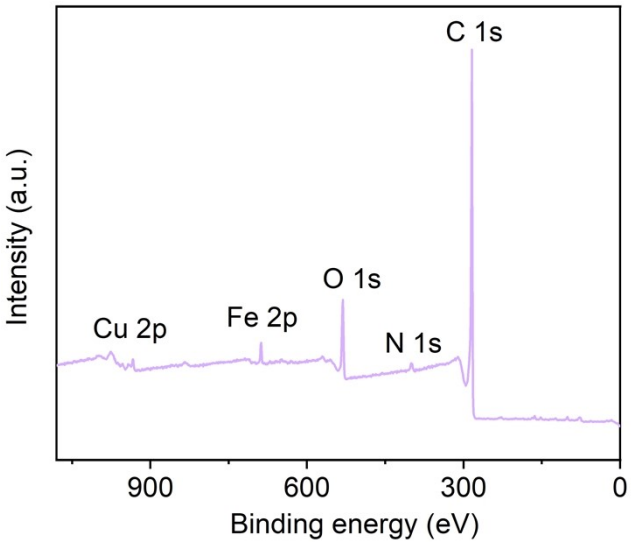

Fig. S27 XPS survey spectrum of Cu-Fe-N-C after NO_3RR.

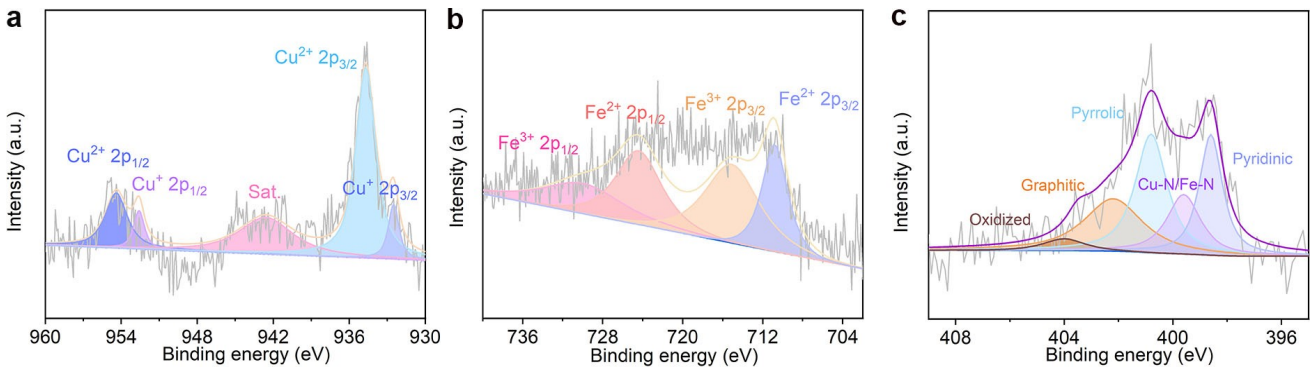

Fig. S28 XPS spectra of Cu-Fe-N-C in the (a) Cu 2p region, (b) Fe 2p region, and (c) N 1s region after NO_3RR.

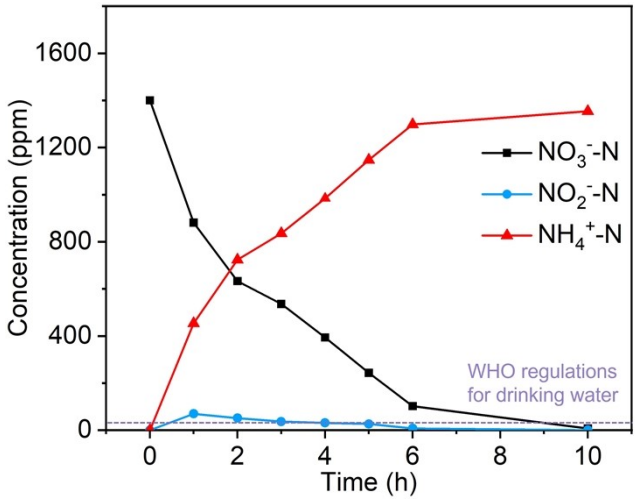

Fig. S29 Time-dependent concentration change of NO_3^--N, NO_2^--N, and NH_4^+-N in the electrolytes for Cu-Fe-N-C**.**

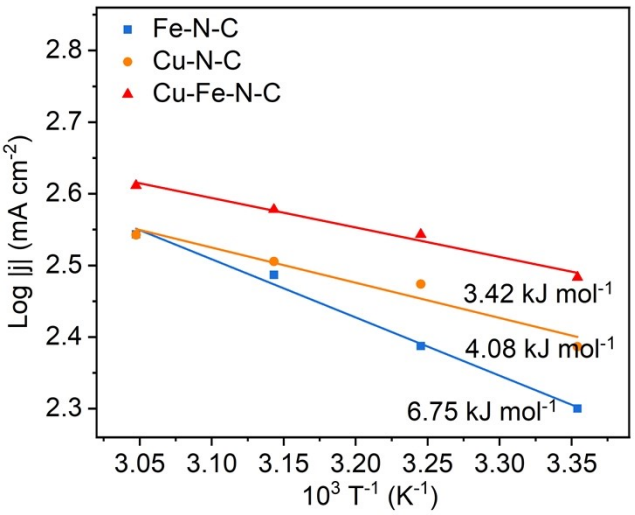

Fig. S30 The Arrhenius plots of the kinetic current at −0.8 V vs. RHE in 1M KOH + 0.1 M KNO_3.

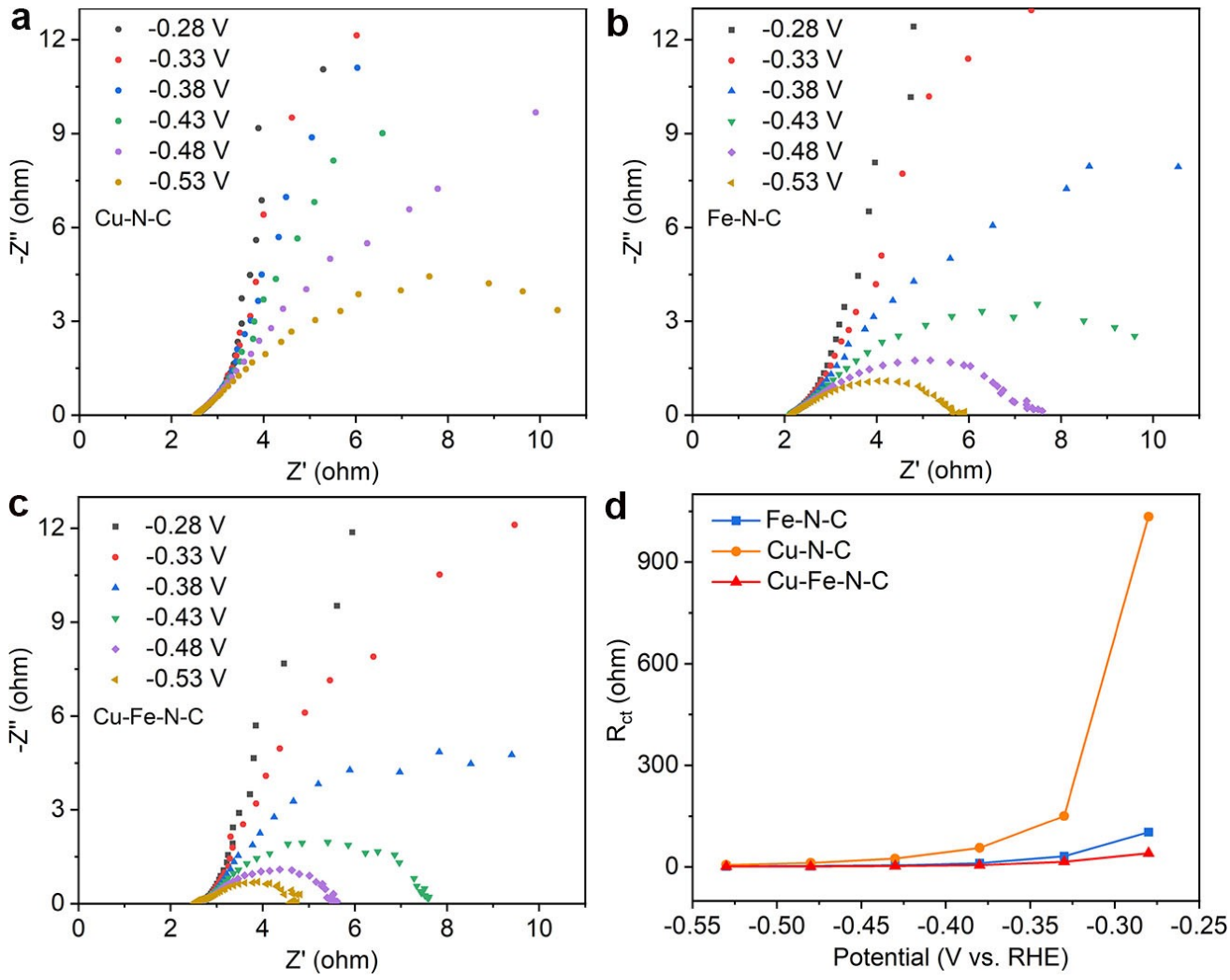

Fig. S31 The electrochemical impedance spectroscopy (EIS) Nyquist plots of (a) Cu-N-C, (b) Fe-N-C, and (c) Cu-Fe-N-C in 1 M KOH at different potentials. (d) The comparison of R_{ct} for the catalysis above in 1 M KOH.

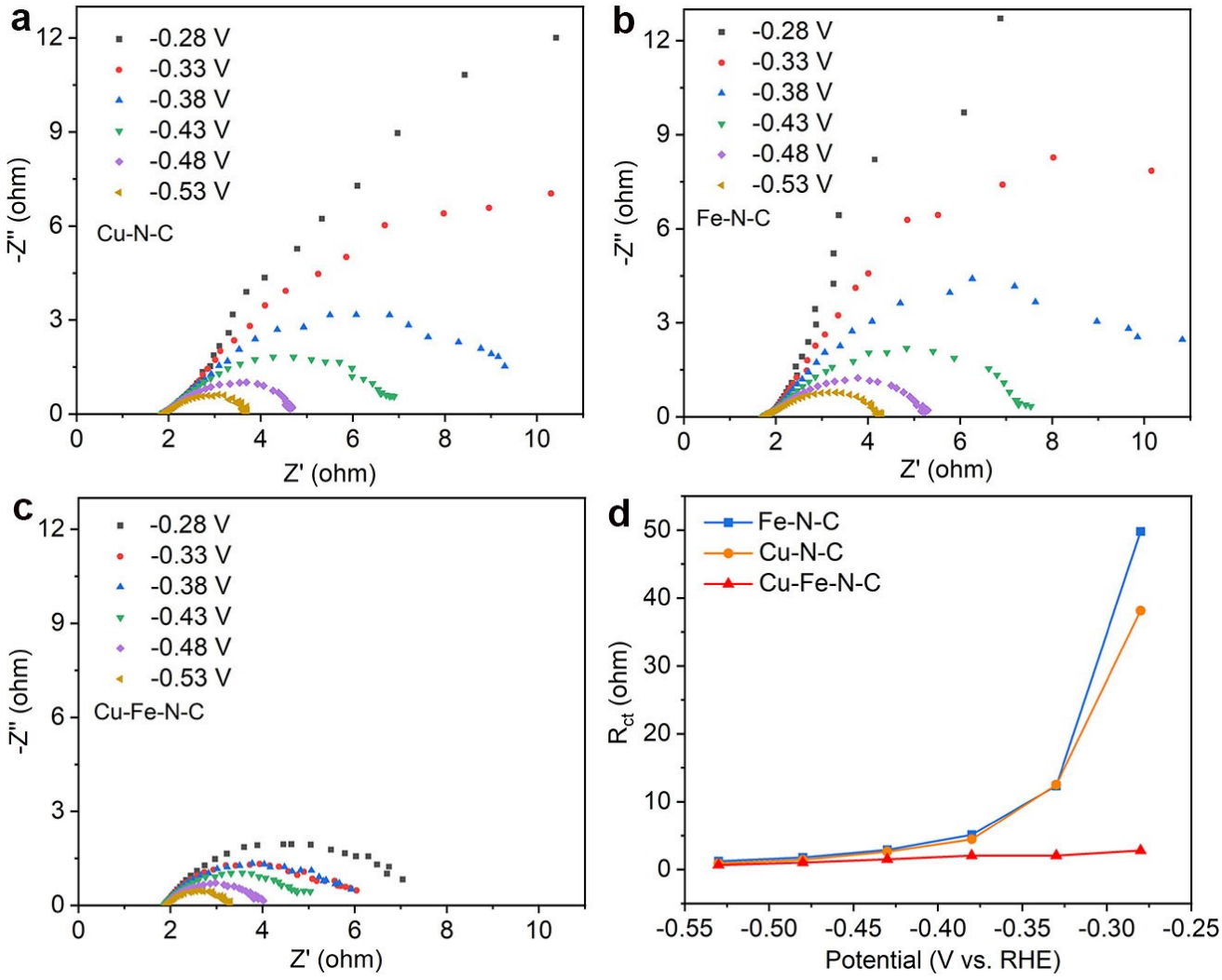

Fig. S32 The electrochemical impedance spectroscopy (EIS) Nyquist plots of (a) Cu-N-C, (b) Fe-N-C, and (c) Cu-Fe-N-C in 1 M KOH with 0.1 M KNO_3 at different potentials. (d) The comparison of R_{ct} for the catalysis above in 1 M KOH with 0.1 M KNO_3.

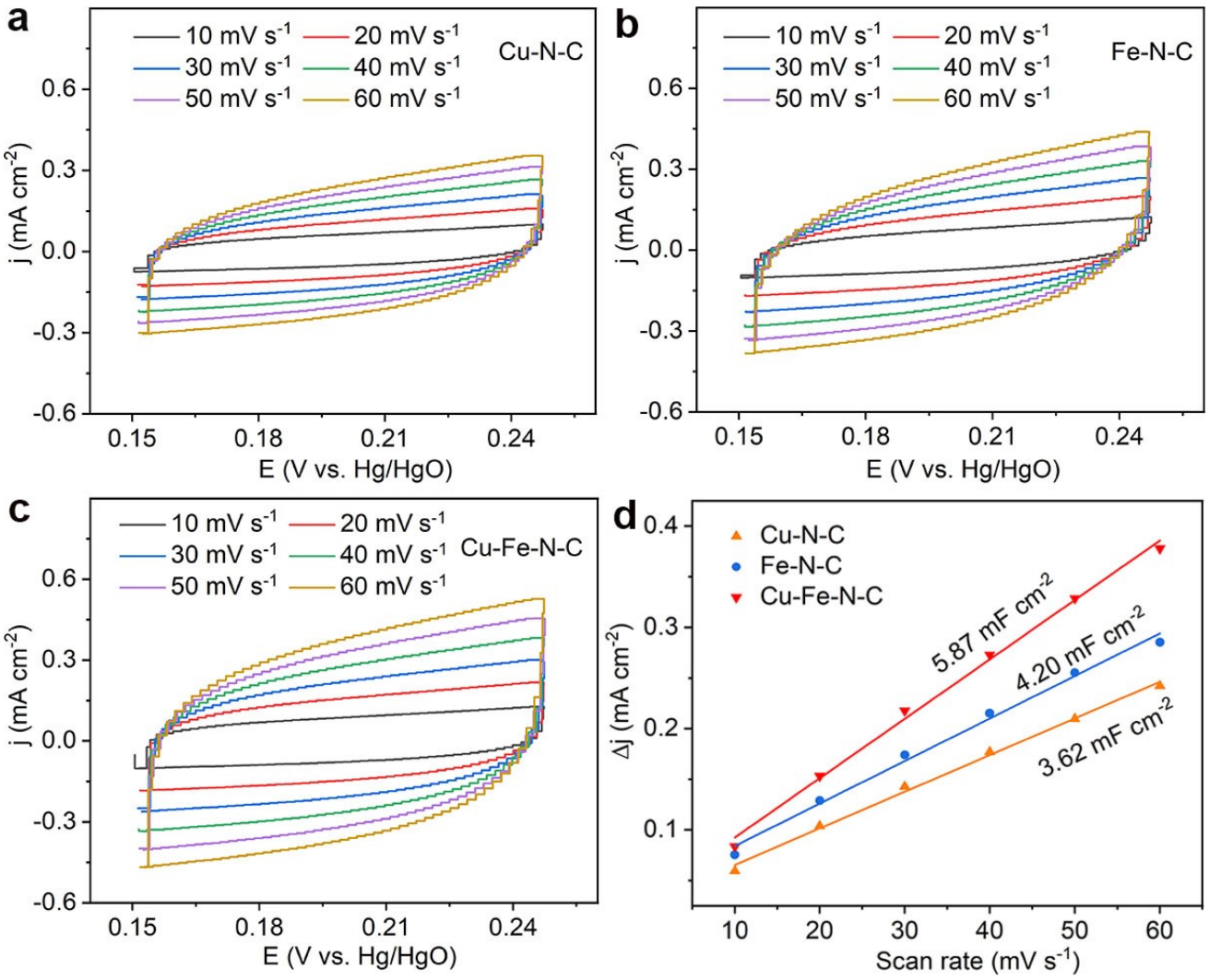

Fig. S33 Cyclic voltammograms (CV) profiles obtained on the (a) Cu-N-C, (b) Fe-N-C, and (c) Cu-Fe-N-C. (d) The determination of double layer capacitance for catalysts.

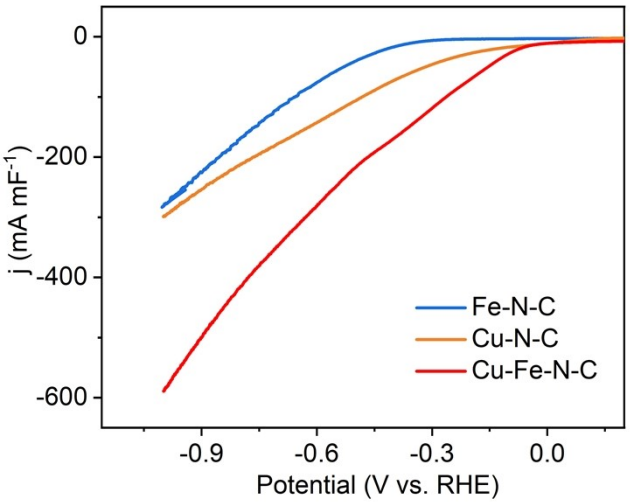

Fig. S34 Double layer capacitance normalized LSV curves of Cu-N-C, Fe-N-C, and Cu-Fe-N-C.

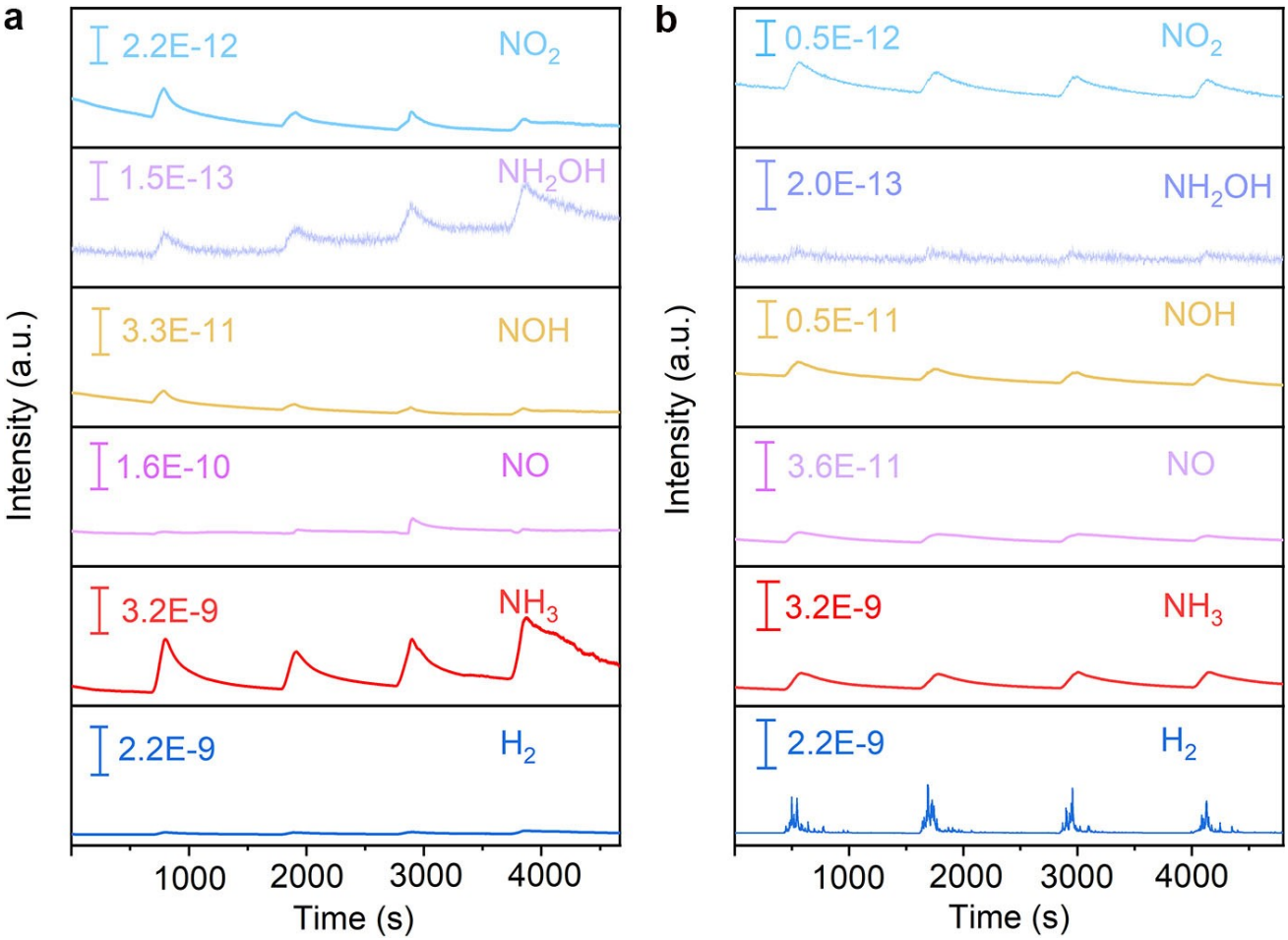

Fig. S35 Electrochemical online DEMS of (a) Cu-N-C and (b) Fe-N-C

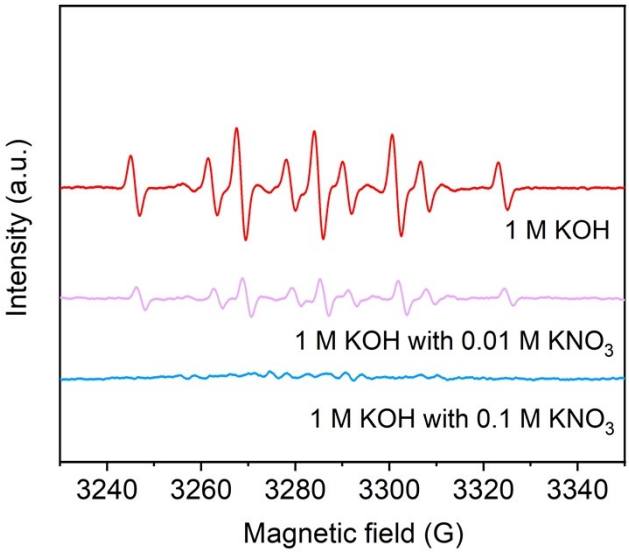

Fig. S36 EPR spectra of Cu-Fe-N-C catalyzed NO_3RR solutions with different concentrations of KNO_3.

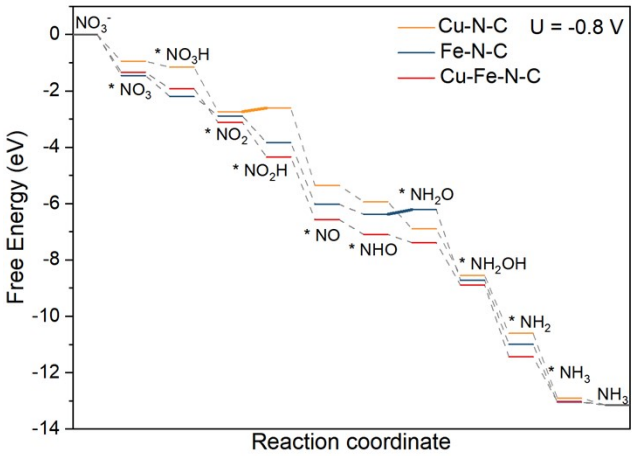

Fig. S37 Free energy profiles of NH_3 formation from NO_3^- reduction on Cu-N-C, Fe-N-C, and Cu-Fe-N-C at -0.8 V vs. RHE.

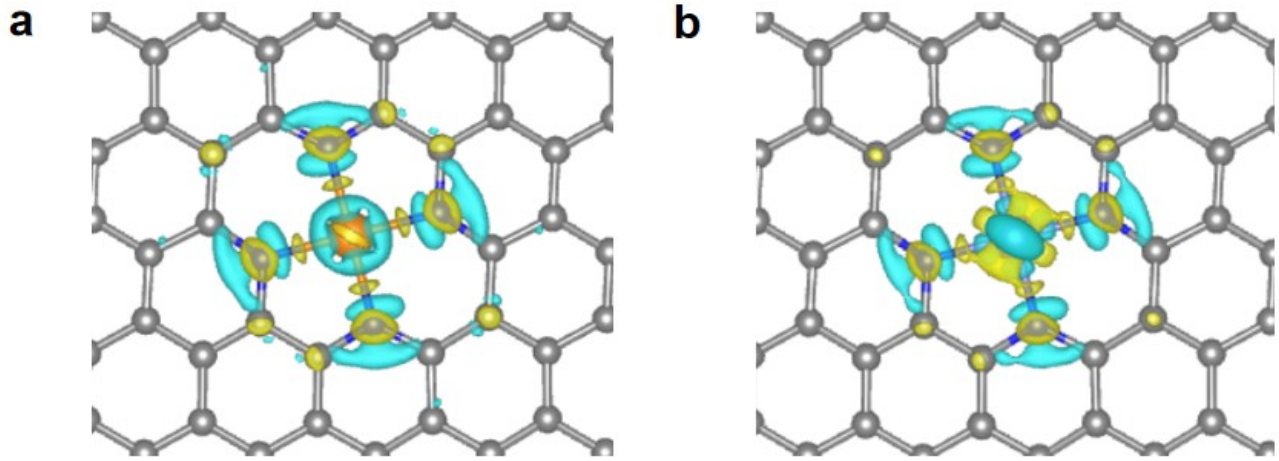

Fig. S38 Differential charge density at the (a) Cu-N-C and (b) Fe-N-C surface (cyan and yellow represent charge depletion and accumulation, respectively).

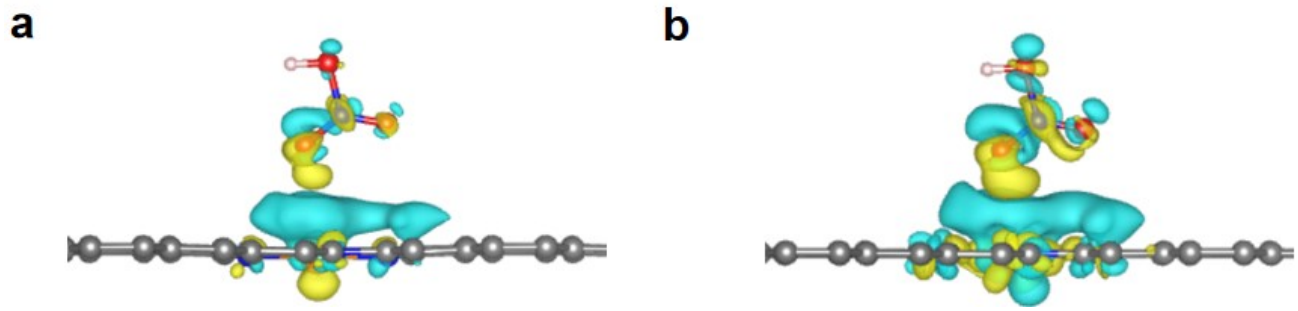

Fig. S39 Differential charge density of *NO_3H on the (a) Cu-N-C and (b) Fe-N-C surface, respectively (cyan and yellow represent charge depletion and accumulation, respectively).

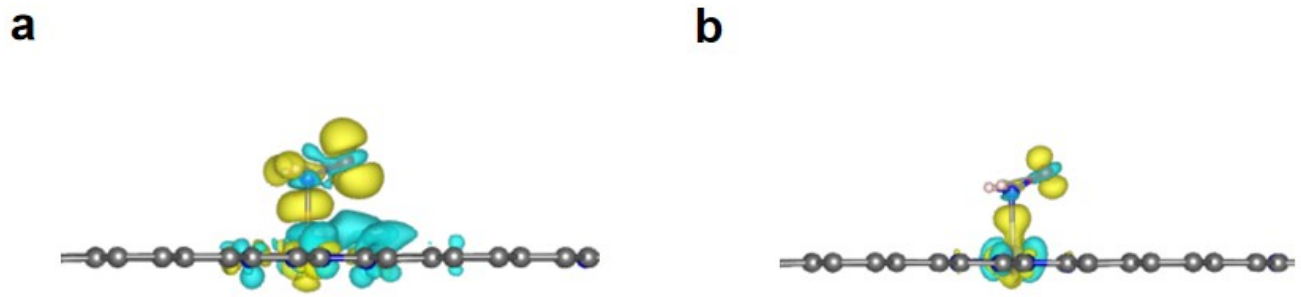

Fig. S40 Differential charge density of *NH_2O on the (a) Cu-N-C and (b) Fe-N-C surface, respectively (cyan and yellow represent charge depletion and accumulation, respectively).

Table S1 EXAFS fitting parameters at the Cu K-edge for various samples

Sample	shell	CN[a]	R[b](Å)	σ²[c](Å²)	ΔE$_0$[d](eV)	R factor
Cu-N-C	Cu-N	4.2±0.2	1.97±0.01	0.0058	4.2±0.9	0.0021
Cu-Fe-N-C	Cu-N	2.9±0.1	1.93±0.01	0.0062	-5.5±1.2	0.0041
	Cu-Fe	1.0±0.1	2.57±0.01	0.0099		

[a]*CN*: coordination numbers; [b]*R*: bond distance; [c]σ^2: Debye-Waller factors; [d]ΔE_0: the inner potential correction. R factor: goodness of fit.

Table S2 EXAFS fitting parameters at the Fe K-edge for various samples

Sample	shell	CN[a]	R[b](Å)	σ^{2c}(Å^2)	ΔE_0[d](eV)	R factor
Fe-N-C	Fe-N	4.2±0.2	1.97±0.01	0.0098	-2.6±1.7	0.0014
Cu-Fe-N-C	Fe-N	3.1±0.1	1.97±0.01	0.0096	-3.7±0.6	0.0003
	Cu-Fe	1.0±0.1	2.58±0.01	0.0123		

[a]*CN*: coordination numbers; [b]*R*: bond distance; [c]σ^2: Debye-Waller factors; [d] ΔE_0: the inner potential correction. R factor: goodness of fit.

Table S3 Comparison of the electrocatalytic NO_3RR performance for NH_3 production of Cu-Fe-N-C with reported catalysts.

Catalyst	Electrolyte	NH_3 yield rate	FE (%)	Ref.
Cu-Fe-N-C	**1 M KOH with 0.1 M NO_3^-**	**1.22 mmol h^{-1} cm^{-2}**	**95.08**	**This work**
Cu-cis-N_2O_2 SAC	0.5 M Na_2SO_4 with 1000 ppm KNO_3	27.84 mg h^{-1} cm^{-2}	88.46	11
Cu-N-C SAC	0.1 M KOH with 0.1 M KNO_3	4.5 mg h^{-1} cm^{-2}	84.7	12
Fe SAC	0.1 M K_2SO_4 with 0.5 M KNO_3	0.46 mmol h^{-1} cm^{-2}	~75	13
Fe-N/P-C	0.1 M KOH + 0.1 M KNO_3	5849.38 μg h^{-1} mg_{cat}^{-1}	90.28	14
Single-atom Ru sites	1 M KOH with 0.5 M NO_3^-	0.15 mmol h^{-1} cm^{-2}	72.8	15
Co-SACs	0.02 M Na_2SO_4 with 100 mg/L NO_3^-	0.433 mg h^{-1} cm^{-2}	92	16
Fe/Cu-NG	1 M KOH with 0.1 M KNO_3	1.08 mmol h^{-1} mg^{-1}	92.51	17
Cu@Th-BPYDC	1 M KOH with 0.1 M NO_3^-	0.2253 mmol h^{-1} cm^{-2}	92.5	18
Cu/PTCDA	0.1 PBS with 500 ppm NO_3^-	0.0515 mmol h^{-1} cm^{-2}	77	19
pCuO-5	0.05 M H_2SO_4 with 0.05 M KNO_3	0.292 mmol h^{-1} cm^{-2}	80	20
Cu nanosheet	0.1 M KOH with 10 mM NO_3^-	0.0046 mmol h^{-1} cm^{-2}	99.7	21
Cu/Cu_2O	0.5 M Na_2SO_4 with 14.3 mM NO_3^-	0.245 mmol h^{-1} cm^{-2}	95.8	22
Cu@NF	1 M KOH with 200 ppm NO_3^-	0.252 mmol h^{-1} cm^{-2}	96.6	23
Rh@Cu	0.1 M Na_2SO_4 with 0.1 M KNO_3	1.27 mmol h^{-1} cm^{-2}	93	24
Fe-cyano NSs	1 M KOH with 0.1 M KNO_3	42.1 mg h^{-1} mg_{cat}^{-1}	90	25
Co/CoO NSAS on Ni foam	0.1 M Na_2SO_4 with 200 ppm NO_3^-	0.1944 mmol h^{-1} cm^{-2}	~93.8	26
Pd (111)	0.1 M Na_2SO_4 with 50 ppm NO_3^-	0.5485 mmol h^{-1} cm^{-2}	79.91	27
In-S-G	1 M KOH with 0.1 M NO_3^-	220 mmol h^{-1} g^{-1}	75	28
TiO_{2-x}	0.5 M Na_2SO_4 with 50 ppm NO_3^-	0.045 mmol h^{-1} mg^{-1}	85	29
Bi-X_{red}	1 M KOH with 0.5 M KNO_3	46.5 g h^{-1} g_{cat}^{-1}	90.6	30
Ni_3B@$NiB_{2.74}$	0.1 M KOH with 10 mM NO_3^-	0.1071 mmol h^{-1} cm^{-2}	98.7	31
PCNV-600	0.5 M Na_2SO_4 with 100 ppm NO_3^--N	0.03262 $mmol^{-1}$ g^{-1} h^{-1}	89.96	32
Cu plates	1 M KOH + 0.5 M KNO_3	3.14 mmol h^{-1} cm^{-2}	75	33

PdCuCo MEA metallene	1 M KOH + 0.1 M KNO_3	458.9 mg h^{-1} mg_{cat}^{-1}	75.4	34
n-HEA	0.2 M K_2SO_4 + 50 mM KNO_3	0.52 mg h^{-1} cm^{-2}	95.23	35
Co_1-P/NPG	0.5 M K_2SO_4 + 0.1 M KNO_3	8.6 mg h^{-1} mg_{cat}^{-1}	93.8	36
PdCu bimetallene	0.5 M K_2SO_4 + 0.1 M KNO_3	73.7 mg h^{-1} mg_{cat}^{-1}	90.9	37
Mn-$Co(OH)_2$	0.5 M K_2SO_4 + 0.1 M KNO_3	1.12 mmol cm^{-2} h^{-1}	98.9	38
RhNi@Rh BMLs	100 mM $HClO_4$ +50 mM KNO_3	13.4 mg h^{-1} mg_{cat}^{-1}	98.5	39
Pd-Cl/Cu_2O	1 M KOH + 56 mM KNO_3	30.1 mg h^{-1} cm^{-2}	99.2	40
Co-B@CoO_x	0.5 M Na_2SO_4 + 100 ppm NO_3-N	0.96 mg h^{-1} cm^{-2}	86.82	41
PR-CuNC	0.1 M KOH + 0.1 M KNO_3	130.71 mg h^{-1} mg_{cu}^{-1}	94.61	42

Table S4 E_d analysis of the constructed Cu-Fe-N-C, Cu-N-C, and Fe-N-C structures models (E_d represents the d-band center).

	E_d(Cu)	E_d(Fe)
Cu-Fe-N-C	-3.076	0.811
Cu-N-C	-3.524	-
Fe-N-C	-	0.214

Table S5 Bader charge analysis of the constructed Cu-Fe-N-C, Cu-N-C, and Fe-N-C structures models (q represents the total charge).

	q_{Cu} (e)	q_{Fe} (e)
Cu-Fe-N-C	16.44	12.90
Cu-N-C	16.17	-
Fe-N-C	-	12.92

References

1. V. I. Anisimov, F. Aryasetiawan and A. I. Lichtenstein, *J. Phys.: Condens. Matter.*, 1997, **9**, 767-808.
2. V. I. Anisimov, J. Zaanen and O. K. Andersen, *Phys. Rev. B.*, 1991, **44**, 943-954.
3. P. E. Blochl, *Phys. Rev. B.*, 1994, **50**, 17953-17979.
4. L. B. Hansen and J. K. Nørskov, *Phys. Rev. B.*, 1999, **59**, 7413.
5. S. Grimme, S. Ehrlich and L. Goerigk, *J. Comput. Chem.*, 2011, **32**, 1456-1465.
6. S. Grimme, J. Antony, S. Ehrlich and H. Krieg, *J Chem Phys*, 2010, **132**, 154104.
7. K. Liu, J. Fu, Y. Lin, T. Luo, G. Ni, H. Li, Z. Lin and M. Liu, *Nat. Commun.*, 2022, **13**, 2075.
8. Z. He, X. Liu, M. Zhang, L. Guo, M. Ajmal, L. Pan, C. Shi, X. Zhang, Z.-F. Huang and J.-J. Zou, *J. Energy Chem.,* 2023, **85**, 570-580.
9. S. Guo, K. Heck, S. Kasiraju, H. Qian, Z. Zhao, L. C. Grabow, J. T. Miller and M. S. Wong, *ACS Catal.*, 2017, **8**, 503-515.
10. X. Zhang, X. Liu, Z.-F. Huang, L. Guo, L. Gan, S. Zhang, M. Ajmal, L. Pan, C. Shi, X. Zhang, G. Yang and J.-J. Zou, *ACS Catal.*, 2023, **13**, 14670-14679.
11. X. F. Cheng, J. H. He, H. Q. Ji, H. Y. Zhang, Q. Cao, W. J. Sun, C. L. Yan and J. M. Lu, *Adv. Mater.*, 2022, **34**, e2205767.
12. J. Yang, H. Qi, A. Li, X. Liu, X. Yang, S. Zhang, Q. Zhao, Q. Jiang, Y. Su, L. Zhang, J. F. Li, Z. Q. Tian, W. Liu, A. Wang and T. Zhang, *J. Am. Chem. Soc.*, 2022, **144**, 12062-12071.
13. Z. Y. Wu, M. Karamad, X. Yong, Q. Huang, D. A. Cullen, P. Zhu, C. Xia, Q. Xiao, M. Shakouri, F. Y. Chen, J. Y. T. Kim, Y. Xia, K. Heck, Y. Hu, M. S. Wong, Q. Li, I. Gates, S. Siahrostami and H. Wang, *Nat. Commun.*, 2021, **12**, 2870.
14. J. Xu, S. Zhang, H. Liu, S. Liu, Y. Yuan, Y. Meng, M. Wang, C. Shen, Q. Peng, J. Chen, Xiaoyang Wang, K. L. Li Song and W. Chen, *Angew. Chem., Int. Ed.*, **62**, e202308044.
15. Z. Ke, D. He, X. Yan, W. Hu, N. Williams, H. Kang, X. Pan, J. Huang, J. Gu and X. Xiao, *ACS Nano*, 2023, **17**, 3483-3491.
16. J. Li, M. Li, N. An, S. Zhang, Q. Song, Y. Yang, J. Li and X. Liu, *PANS*, 2022, **119**, e2123450119.
17. S. Zhang, J. Wu, M. Zheng, X. Jin, Z. Shen, Z. Li, Y. Wang, Q. Wang, X. Wang, H. Wei, J. Zhang, P. Wang, S. Zhang, L. Yu, L. Dong, Q. Zhu, H. Zhang and J. Lu, *Nat. Commun.*, 2023, **14**, 3634.
18. Z. Gao, Y. Lai, Y. Tao, L. Xiao, L. Zhang and F. Luo, *ACS Cent. Sci.*, 2021, **7**, 1066-1072.
19. G.-F. Chen, Y. Yuan, H. Jiang, S.-Y. Ren, L.-X. Ding, L. Ma, T. Wu, J. Lu and H. Wang, *Nat. Energy*, 2020, **5**, 605-613.
20. R. Daiyan, T. Tran-Phu, P. Kumar, K. Iputera, Z. Tong, J. Leverett, M. H. A. Khan, A. Asghar Esmailpour, A. Jalili, M. Lim, A. Tricoli, R.-S. Liu, X. Lu, E. Lovell and R. Amal, *Energy Environ. Sci.*, 2021, **14**, 3588-3598.
21. X. Fu, X. Zhao, X. Hu, K. He, Y. Yu, T. Li, Q. Tu, X. Qian, Q. Yue, M. R. Wasielewski and Y. Kang, *Appl. Mater. Today*, 2020, **19**, 100620.
22. Y. Wang, W. Zhou, R. Jia, Y. Yu and B. Zhang, *Angew. Chem. Int. Ed.*, 2020, **59**, 5350-5354.
23. J. Li, J. Gao, T. Feng, H. Zhang, D. Liu, C. Zhang, S. Huang, C. Wang, F. Du, C. Li and C. Guo, *J. Power Sources*, 2021, **511**, 230463.
24. H. Liu, X. Lang, C. Zhu, J. Timoshenko, M. Ruscher, L. Bai, N. Guijarro, H. Yin, Y. Peng, J. Li, Z. Liu, W. Wang, B. R. Cuenya and J. Luo, *Angew. Chem. Int. Ed.*, 2022, **61**, e202202556.
25. Z. Fang, Z. Jin, S. Tang, P. Li, P. Wu and G. Yu, *ACS Nano*, 2022, **16**, 1072-1081.
26. Y. Yu, C. Wang, Y. Yu, Y. Wang and B. Zhang, *Sci. Chi. Chem*, 2020, **63**, 1469-1476.
27. Y. Han, X. Zhang, W. Cai, H. Zhao, Y. Zhang, Y. Sun, Z. Hu, S. Li, J. Lai and L. Wang, *J. Colloid Interface Sci.*, 2021, **600**, 620-628.
28. F. Lei, W. Xu, J. Yu, K. Li, J. Xie, P. Hao, G. Cui and B. Tang, *Chem. Eng. J.*, 2021, **426**, 131317.
29. R. Jia, Y. Wang, C. Wang, Y. Ling, Y. Yu and B. Zhang, *ACS Catal.*, 2020, **10**, 3533-3540.
30. N. Zhang, J. Shang, X. Deng, L. Cai, R. Long, Y. Xiong and Y. Chai, *ACS Nano*, 2022, **16**, 4795-4804.
31. L. Li, C. Tang, X. Cui, Y. Zheng, X. Wang, H. Xu, S. Zhang, T. Shao, K. Davey and S. Z. Qiao, *Angew. Chem. Int. Ed.*, 2021, **60**, 14131-14137.
32. Y. Huang, J. Long, Y. Wang, N. Meng, Y. Yu, S. Lu, J. Xiao and B. Zhang, *ACS Appl. Mater. Interfaces*, 2021, **13**, 54967-54973.
33. L. Zhou, X. Chen, S. Zhu, K. You, Z. J. Wang, R. Fan, J. Li, Y. Yuan, X. Wang, J. Wang, Y. Chen, H. Jin, S. Wang and J. J. Lv, *Angew. Chem. Int. Ed.*, 2024, **63**, e202401924.
34. Y. Zhou, L. Zhang, M. Wang, Z. Zhu, N. Li, T. Qian, C. Yan and J. Lu, *ACS Catal.*, 2024, **14**, 7907-7916.
35. R. Zhang, Y. Zhang, B. Xiao, S. Zhang, Y. Wang, H. Cui, C. Li, Y. Hou, Y. Guo, T. Yang, J. Fan and C. Zhi, *Angew. Chem. Int. Ed.*, 2024, e202407589.
36. J. Ni, J. Yan, F. Li, H. Qi, Q. Xu, C. Su, L. Sun, H. Sun, J. Ding and B. Liu, *Adv. Energy Mater.*, 2024, 2400065.
37. Y. Zhou, L. Zhang, Z. Zhu, M. Wang, N. Li, T. Qian, C. Yan and J. Lu, *Angew. Chem. Int. Ed.*, 2024, **63**, e202319029.
38. S. Liang, X. Teng, H. Xu, L. Chen and J. Shi, *Angew. Chem. Int. Ed.*, 2024, **63**, e202400206.
39. W. Zhong, Q. L. Hong, X. Ai, C. Zhang, F. M. Li, X. F. Li and Y. Chen, *Adv. Mater.*, 2024, **36**, e2314351.
40. W. Liao, J. Wang, G. Ni, K. Liu, C. Liu, S. Chen, Q. Wang, Y. Chen, T. Luo, X. Wang, Y. Wang, W. Li, T. S. Chan, C. Ma, H. Li, Y. Liang, W. Liu, J. Fu, B. Xi and M. Liu, *Nat. Commun.*, 2024, **15**, 1264.
41. X. Zhu, C. Ma, Y.-C. Wang, K. Qu, L. Song, J. Wang, Y. Gong, X. Liu, J. Zhang, Q. Lu and A.-L. Wang, *Energy Environ. Sci.*, 2024, **17**, 2908-2920.
42. Y. Liu, W. Qiu, P. Wang, R. Li, K. Liu, K. M. Omer, Z. Jin and P. Li, *Appl. Catal. B-Environ.*, 2024, **340**, 123228.